Digitized Theses   Digitized Special Collections

2011

Design of Orexin Based Imaging Agents

Zhu Lin

Recommended Citation

Design of Orexin Based Imaging Agents

(Spine title: Design of Orexin Based Imaging Agents)

(Thesis format: Monograph)

by

Zhu Lin

Graduate Program in Chemistry

A thesis submitted in partial fulfillment

of the requirements for the degree of

Master of Chemistry

The School of Graduate and Postdoctoral Studies

The University of Western Ontario

London, Ontario, Canada

THE UNIVERSITY OF WESTERN ONTARIO
SCHOOL OF GRADUATE AND POSTDOCTORAL STUDIES

CERTIFICATE OF EXAMINATION

Supervisor

_____
Dr. Leonard G. Luyt

Examiners

_____
Dr. Mel C. Usselman

_____
Dr. Brain L. Pagenkopf

_____
Dr. Donna Goldhawk

The thesis by

Zhu Lin

entitled:

Design of Orexin Based Imaging Agents

is accepted in partial fulfillment of the
requirements for the degree of
Master of Chemistry

Date_____   _____
                                    Chair of the Thesis Examination Board

Abstract

Orexin A (33 amino acids) and orexin B (28 amino acids) are two naturally occurring ligands of the G-protein coupled receptor: orexin receptor 1 (OX_1R) and orexin receptor 2 (OX_2R). Based on the expression of OX_1R in colon cancer cells, gallium-68 labelled orexin A (15-33) and orexin B (6-28) were developed as potential PET imaging agents targeting colon cancer cells. Orexin A (15-33) and orexin B (6-28) were synthesized by Fmoc solid phase peptide synthesis (SPPS). A bifunctional chelator 1,4,7,10-tetra azacyclo dodecane- *N,N',N",N"'*-tetraacetic acid (DOTA) was used to attach gallium-68 to orexin A (15-33) and orexin B (6-28). A linker aminohexanoic acid (Ahx) was incorporated between the targeting peptide sequence and ^{68}Ga-DOTA complex to reduce the bulky effect of the imaging label on the binding affinities. It was determined that the IC_{50} values of Ga-DOTA-Ahx-orexin A (15-33) and Ga-DOTA-Ahx-orexin B (6-28) were 629 nM and 168 nM respectively. In order to evaluate the binding affinities in cells, orexin A (13-33) and orexin B (6-28) were also labeled with fluorescein isothiocyanate (FITC) allowing for fluorescence microscopy studies. Besides orexin A and orexin B analogues, a potential orexin receptor antagonist was developed as a potential imaging agent as well and preliminary synthetic steps were undertaken. This antagonist was proposed to be labelled with fluorine-18 to form the compound $[^{18}F]$(4-fluoro-phenyl)-(4-quinozolin-2-yl-[1,4]diazepan-1-yl)-methanone as an imaging agent targeting colon cancer cells.

Abstract

Orexin A (33 amino acids) and orexin B (28 amino acids) are two naturally occurring ligands of the G-protein coupled receptor: orexin receptor 1 (OX_1R) and orexin receptor 2 (OX_2R). Based on the expression of OX_1R in colon cancer cells, gallium-68 labelled orexin A (15-33) and orexin B (6-28) were developed as potential PET imaging agents targeting colon cancer cells. Orexin A (15-33) and orexin B (6-28) were synthesized by Fmoc solid phase peptide synthesis (SPPS). A bifunctional chelator 1,4,7,10-tetra azacyclo dodecane- *N,N',N'',N'''*-tetraacetic acid (DOTA) was used to attach gallium-68 to orexin A (15-33) and orexin B (6-28). A linker aminohexanoic acid (Ahx) was incorporated between the targeting peptide sequence and ^{68}Ga-DOTA complex to reduce the bulky effect of the imaging label on the binding affinities. It was determined that the IC_{50} values of Ga-DOTA-Ahx-orexin A (15-33) and Ga-DOTA-Ahx-orexin B (6-28) were 629 nM and 168 nM respectively. In order to evaluate the binding affinities in cells, orexin A (13-33) and orexin B (6-28) were also labeled with fluorescein isothiocyanate (FITC) allowing for fluorescence microscopy studies. Besides orexin A and orexin B analogues, a potential orexin receptor antagonist was developed as a potential imaging agent as well and preliminary synthetic steps were undertaken. This antagonist was proposed to be labelled with fluorine-18 to form the compound [^{18}F](4-fluoro-phenyl)-(4-quinozolin-2-yl-[1,4]diazepan-1-yl)-methanone as an imaging agent targeting colon cancer cells.

Acknowledgements

Table of Contents

List of Tables

List of Figures

List of Schemes

List of Abbreviations

AEEA	[2-[2-Amino ethoxy] ethoxy] acetic acid
Ahx	Amino hexanoic acid
BBN	Bombesin
DCM	Dichloromethane (DCM)
DCE	Dichloroethane
DIPEA	N,N-diisopropylethylamine
DMF	Dimethylformamide
DORA	Orexin receptor antagonist
DOTA	1,4,7,10-Tetraazacyclododecane-1,4,7,10-tetraacetic acid
DTPA	Diethylene triamine pentaacetic acid
EC_{50}	Half maximal effective concentration
ESI-MS	Electrospray ionization-mass spectroscopy
$[^{18}F]FBA$	$[^{18}F]$Fluorobenzoic acid
FDG	Fluorodeoxyglucose
FITC	Fluorescein isothiocyanate
Fmoc	Fluorenylmethyloxycarbonyl
Fmoc-Cl	Fluorenylmethyloxycarbonyl chloride
GPCR	G-protein coupled receptor
HBTU	1-[bis(Dimethylamino)methylene]-1H-benzotriazolium hexafluorophosphate 3-oxide
IC_{50}	Half maximal inhibitory concentration
LC-MS	Liquid chromatography- mass spectroscopy
mCi	Millicurie
MRI	Magnetic resonance imaging
NIR	Near infrared
NMR	Nuclear magnetic resonance
NOTA	1,4,7-Triazacyclononane-1,4,7-triacetic acid

OtBu	*O-tert*-butyl
OX_1R	Orexin receptor 1
OX_2R	Orexin receptor 2
Pbf	2,2,4,6,7-Pentamethyldihydrobenzofuran-5-sulphonyl
PEG	Polyethylene glycol
PET	Positron emission tomography
RP-HPLC	Reverse phase-high performance liquid chromatography
S_0	Ground electronic state
S_1	The first excited electronic state
S_2	The second excited electronic state
$[^{18}F]SFB$	*N*-succinimidyl 4-$[^{18}F]$fluoromethyl benzoate
SORA	Selective orexin receptor antagonist
SPECT	Single-photon emission computed tomography
SPPS	Solid phase peptide synthesis
SST	Somatostatin
TBME	Tert-butyl methyl ether
tBu	*Tert*-butyl
TEMPO	2,2,6,6-Tetramethylpiperidine-1-oxyl
TFA	Trifluoroacetic acid
THF	Tetrahydrofuran
TIS	Triisopropylsilane
TMS	Trimethylsilane
Trt	Trityl
TSTU	O-(*N*-succinimidyl)-N,N,N',N'-tetramethyluronium tetrafluoroborate
UV	Ultraviolet
p	Proton
n	Neutron
β^+	Positron
ν	Neutrino

Chapter 1 Introduction

1.1 Molecular Imaging

Molecular imaging is the combination of molecular and cellular biology and *in vivo* imaging. It is a non-invasive way to visualize cellular functions and characterize biological processes in living organisms.[1] Molecular imaging has become very attractive in recent years, because it has great potential in the diagnosis of disease, such as cancer. Compared with traditional diagnosis, molecular imaging may detect the disease earlier and more accurately. Molecular imaging is dependent on an imaging device and an imaging probe (imaging agent). Once an imaging probe is injected into a body, it accumulates in the specific cells such as tumor cells, or binds to its target which is overexpressed in those specific cells compared to surrounding normal cells. The imaging probe is detected by the corresponding imaging device to create an image of its distribution in the body, which helps analyze the functioning of organs and tissues.

A molecular imaging probe includes two components: targeting component and imaging component, as shown in Figure 1.1. Targeting components can be peptides, small molecules, antibodies, proteins or cells and their responsibility is to identify the target of interest in the body.[2] In order to be visualized *in vivo*, the targeting entity is labelled by different imaging components, such as radionuclides, fluorophores or contrast agents.[2] Normally, the linker is used between the targeting and imaging components to reduce the effect of labelling materials on the interaction of targeting entities and their targets.

1
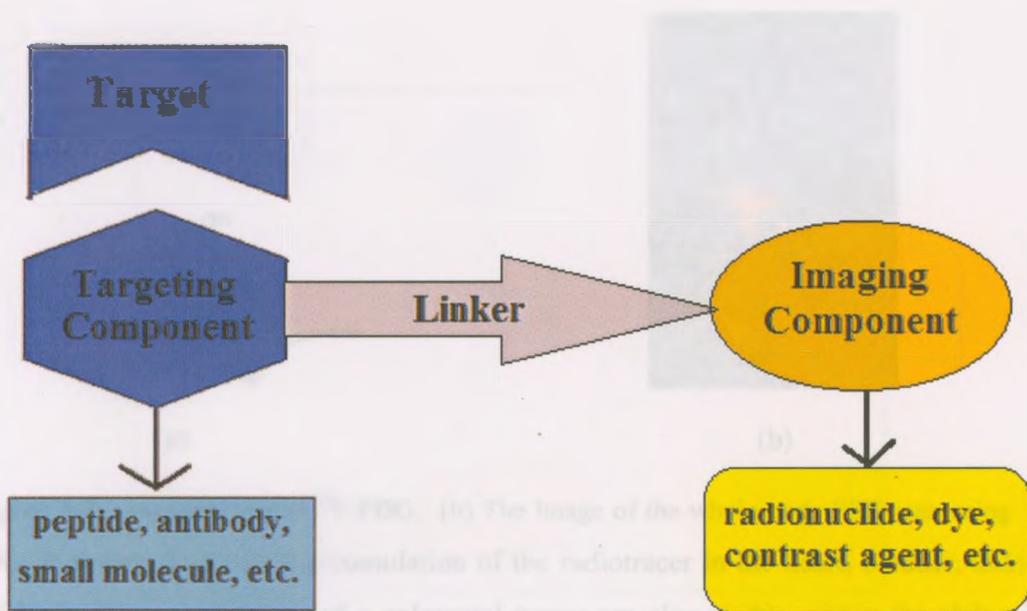
Figure 1.1 General design of molecular imaging probes.

There are many imaging modalities, such as radionuclide imaging and optical imaging. Optical imaging uses fluorescent or luminescent probes emitting visible or near infrared lights. However, the light emitted from fluorophores can only travel a few millimetres at most through tissues, so optical imaging is widely used in cells, skins and small animals, but not in deep tissues. Radionuclide imaging can visualize radionuclide-labelled probes with a very low concentration, but the resolution of the image is low. Based on different labelling radionuclides, radionuclide imaging can be divided into single-photon emission computed tomography (SPECT) imaging and positron emission tomography (PET) imaging. Figure 1.2 shows an example of the whole-body PET imaging with fluorine-18 labelled fluorodeoxyglucose (^{18}F-FDG) as the imaging probe. FDG, an analogue of glucose, is taken up by the organs or cells with high glucose consumption, such as brain, kidney and cancer cells.
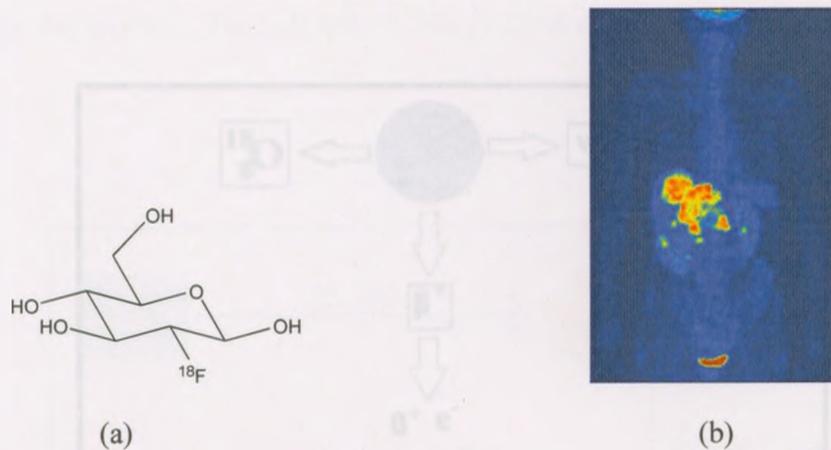
Figure 1.2 (a) Structure of ^{18}F-FDG. (b) The image of the whole-body PET scan using ^{18}F-FDG. It shows the normal accumulation of the radiotracer in the heart, bladder, kidneys and brain. Liver metastases of a colorectal tumor are also visible within the abdominal region of the image.[3]

1.2 Positron Emission Tomography (PET) Imaging

Positron emission tomography is a non-invasive imaging modality using probes labelled with positron emitting radioisotopes, such as ^{68}Ga and ^{18}F. PET was originally developed in the 1960s and PET imaging agents give both qualitative and quantitative measurement of biological processes. Figure 1.3 shows the basic principle of PET imaging.[4] The neutron-deficient nucleus remains stable through the transmutation of a proton (p) into a neutron (n), emitting a positron (β^+) and an electron neutrino (ν). Then the positron travels a short distance and annihilates with an electron from the surrounding environment. The positron and electron annihilate, followed by the emission of two photons of 511 keV 180° apart. The two gamma photons are captured in coincidence by two detectors on the opposite directions. Based on those detected coincidences, a 3D image is produced.
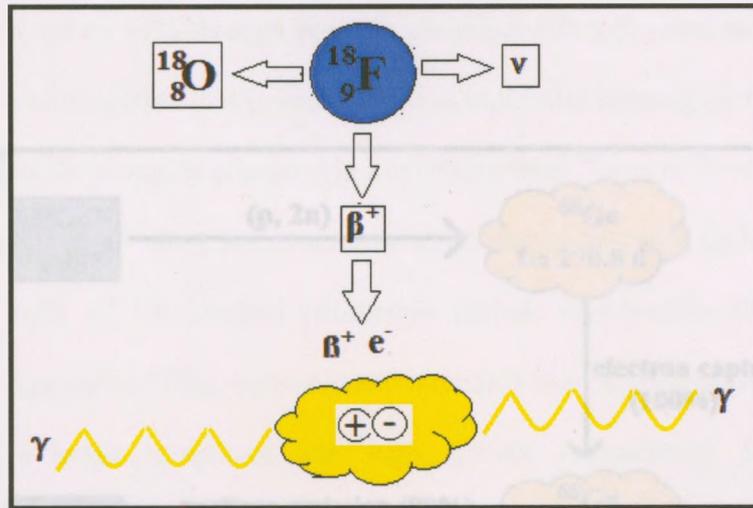
Figure 1.3. The basic principle of PET technique.

1.3 Gallium-68: A Radionuclide for PET Imaging

In PET/SPECT imaging, imaging entities are labelled by radionuclides. Based on their decay type, physical half life, availability and ease of labelling, some radionuclides have preferential characteristics for labelling the imaging agent, including ^{99m}Tc, ^{18}F, and ^{68}Ga.[5] Among those radionuclides, ^{68}Ga may be used to create PET imaging agents. ^{68}Ga decays by positron emission (89%) and electron capture (11%) with a short physical half-life of 68 minutes, capable of minimizing the radiation exposure to subjects.[6] In addition, 68 minutes is also long enough for the radiotracer to reach the target and to get the target image through a PET scan. The major advantage of using ^{68}Ga as a medical isotope is that ^{68}Ga can be produced by a ^{68}Ge/^{68}Ga generator system (Figure 1.4) rather than an on-site based cyclotron system, and is more accessible and more cost-effective. As indicated in Figure 1.4, the parent isotope of ^{68}Ga is ^{68}Ge, which is produced from a gallium target

4

by the (p, 2n) reaction. The half life of ^{68}Ge is 270.8 days, giving a long-lived generator system.
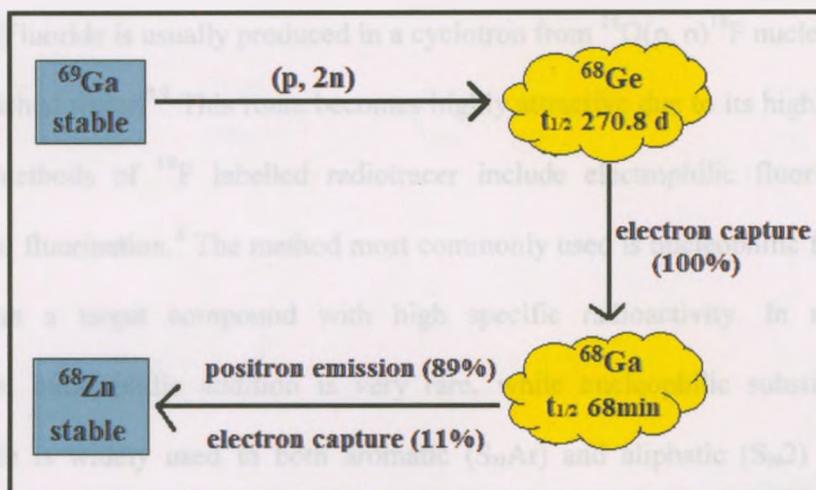
Figure 1.4 Production and decay of ^{68}Ge and ^{68}Ga.[6]

In order to attach ^{68}Ga to the targeting entity, a bifunctional chelator is generally used to link them together, especially in the design of peptide-based imaging probes. Because Ga^{3+} is a hard Lewis acid, it normally complexes with hard Lewis bases to form a thermally stable compound. The ideal chelators should contain oxygen, nitrogen or sulfur donor atoms, such as carboxylate and phosphonate, but also softer functional groups (Figure 1.5).[7]
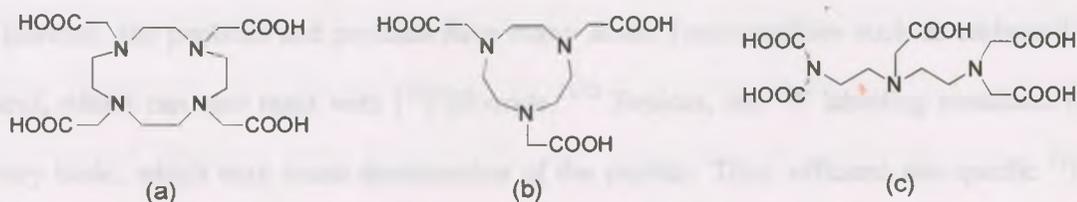
Figure 1.5 Commonly used chelators, (a) DOTA, (b) NOTA, (c) DTPA.

1.4 Fluorine-18: A Radionuclide for PET Imaging

Fluorine-18 decays by 97% through positron emission with a physical half-life of 109.7 minutes. It is a radionuclide that is widely used in molecular imaging by the way of PET scans. [^{18}F]Fluoride is usually produced in a cyclotron from ^{18}O(p, n)^{18}F nuclear reactions on ^{18}O-enriched water.[8,9] This route becomes highly attractive due to its high yield.[8] The synthetic methods of ^{18}F labelled radiotracer include electrophilic fluorination and nucleophilic fluorination.[8] The method most commonly used is nucleophilic fluorination, which gives a target compound with high specific radioactivity. In nucleophilic fluorination, nucleophilic addition is very rare, while nucleophilic substitution with [^{18}F]fluoride is widely used in both aromatic (S_NAr) and aliphatic (S_N2) series. The nucleophilic substitution can be performed directly on a suitable precursor as shown in Scheme 1.1.[10]
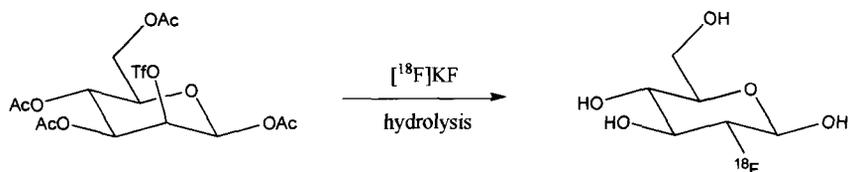
Scheme 1.1 ^{18}F-fluorination and subsequent hydrolysis for the preparation of [^{18}F]FDG via the method of direct nucleophilic substitution.[10]

However, the peptides and proteins have many acidic functionalities such as carboxylic acid, which can also react with [^{18}F]fluoride.[11,12] Besides, the ^{18}F labelling condition is very basic, which may cause denaturation of the peptide. Thus, efficient site-specfic ^{18}F labelling of peptides and proteins has to be carried out by indirect fluorination through suitable prosthetic groups.[13] One of the most suitable prosthetic groups is *N*-succinimidyl

4-[18F]fluoromethyl benzoate ([18F]SFB), which introduces ^{18}F into a peptide via coupling to the amino group or a lysine residue of the peptide.[14] Scheme 1.2 shows the preparation of [18F]SFB and the [18F]fluorination of a peptide via [18F]SFB.
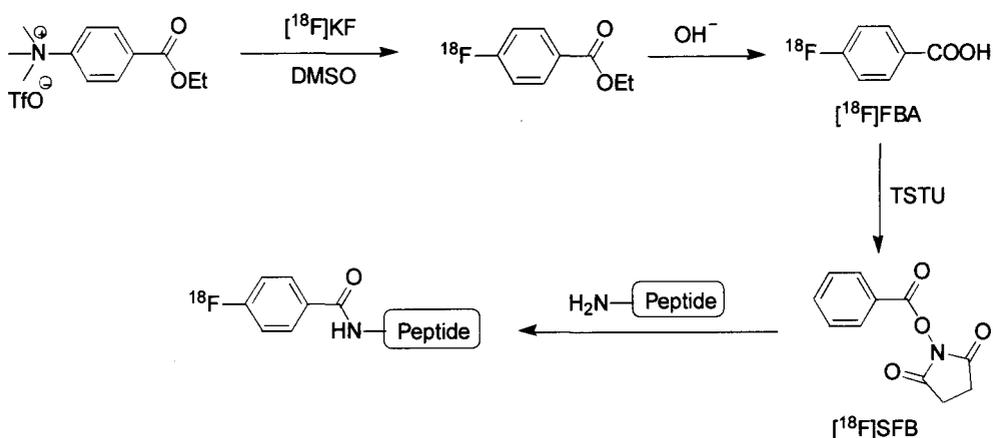
Scheme 1.2   A general procedure for the preparation of ^{18}F-labelled peptides via [18F]SFB with TSTU as the coupling agent. *[18F]FBA*, [18F]fluorobenzoic acid; *[18F]SFB*, *N*-succinimidyl 4-[18F](fluoromethyl) benzoate; *TSTU*, O-(N-succinimidyl)-N,N,N',N'-tetramethyluronium tetrafluoroborate.[13,15]

1.5 Fluorescence Imaging

Fluorescence imaging is based on detecting the fluorescent emission through cells or biological tissues, in which a fluorophore is used to label the targeting entity. When the fluorophore absorbs the light with a specific wavelength, the fluorophore molecule in the ground electronic state (S_0) is excited to the vibrational states in the first (S_1) or second (S_2) excited electronic states (Figure 1.6). Due to collisions with other molecules, the excited molecule loses energy and falls to the lowest vibrational level of excited states. Then the molecule from the lowest excited electronic state returns back to the ground

electronic state, emitting the energy in the form of fluorescence.
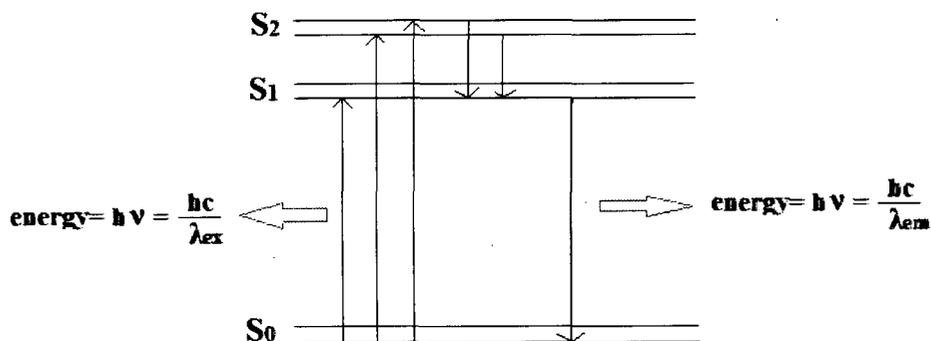
Figure 1.6 Principle of fluorescence spectroscopy.

One of the commonly used fluorophores is fluorescein isothiocyanate (FITC), which is an amine reactive derivative of fluorescein dyes (Figure 1.7). FITC has a maximum excitation wavelength of 495 nm and a maximum emission wavelength of 521 nm. In the design of peptide-based molecular imaging probes, FITC was incorporated to the imaging entity via the reaction between the isothiocyanate functionality of FITC and the amino functionality of the peptide-based targeting entity (Scheme 1.3).

(a)   (b)
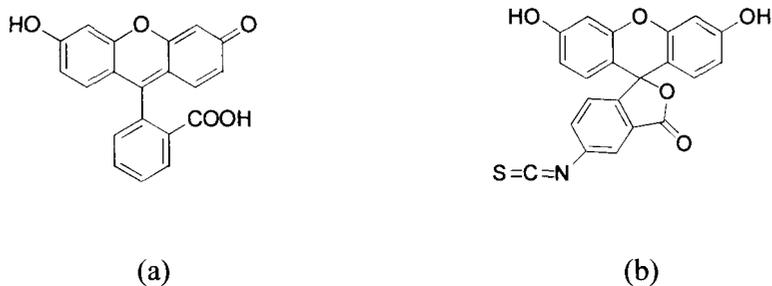
Figure 1.7 (a) The structure of fluorescein. (b) The structure of fluorescein isothiocyanate (FITC).
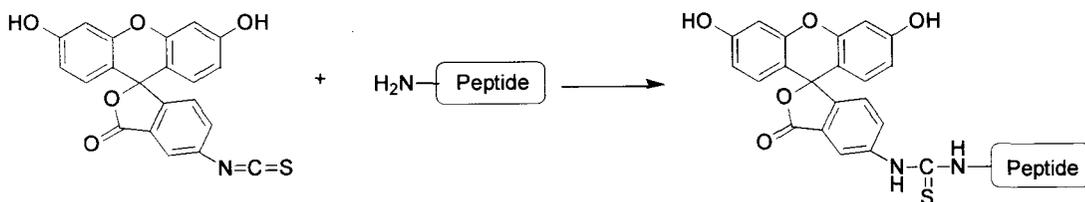
Scheme 1.3 Reaction between FITC and targeting peptides.

1.6 Peptide-based Molecular Imaging Probes

As a product of genes, biologically active peptides play a significant role in the body via specific binding activities with their receptors.[16,17] These receptors are proteins or protein-coupled receptors, such as G-protein coupled receptors (GPCRs). Many of these receptors are overexpressed in certain diseases, especially in some tumor cells.[18] Through binding with their receptors, those naturally occurring peptides can activate or inhibit the corresponding biological processes. Thus, the specific receptor binding of a peptide may provide a way for cancer targeting via peptide-based molecular imaging. As a targeting entity, the peptide can be labelled by different imaging components, such as radionuclides and fluorophores. There are several advantages to use peptides as targeting entities.[16] First of all, specific peptides have high binding affinities with their receptors, which is the prerequisite to screen or monitor certain diseases. Besides, selected peptides are active at nanomolar concentrations with a low molecular weight, so they can be highly taken up by the target receptor and cleared from the blood easily. Also, capillary permeability of peptides is better than that of antibodies, which help them penetrate into the targets efficiently. Finally, peptides have low toxicity and immunogenicity, reducing the possibilities of potential adverse effects.

One of the representative peptide-based imaging probes in clinical study is [68]Ga-[DOTA-Tyr[3]]-octreotide (^{68}Ga-DOTA-TOC), a somatostatin (SST) analogue, which was designed to target neuroendocrine tumor cells (Figure 1.8).[19] SSTs are a family of cyclopeptides inhibiting the secretion of insulin, hormone and glucagon.[20] Somatostatin receptors (SSTrs) are overexpressed in tumors such as breast cancer and neuroendocrine tumors.[21] Based on the targets SSTrs, some potential SST-based imaging probes have been developed such as ^{68}Ga-DOTA-TOC. Clinical study of ^{68}Ga-DOTA-TOC has demonstrated that it is effective for the imaging of neuroendocrine tumors.[22]
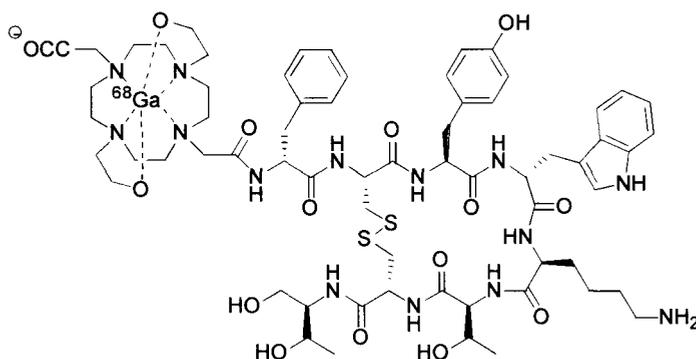
Figure 1.8 Structure of ^{68}Ga-DOTA-TOC.

1.7 Solid Phase Peptide Synthesis

Solid phase peptide synthesis (SPPS) was first developed by Robert Bruce Merrifield in 1963, which earned him the Nobel Prize in 1984.[23] SPPS is a method by which the peptide chain is synthesized on a solid support. The solid support is composed of small solid beads, insoluble yet porous. These solid insoluble beads are modified by linkers, which behave as a reversible linkage between the peptide chain and the solid beads (Figure 1.9).[24] The general principle of SPPS is shown in Figure 1.10.[24] The first amino

acid is attached to the solid support covalently by its carboxyl group. After deprotection, the free N-terminal amine is coupled to the next amino acid. The cycle of deprotection-wash-coupling-wash is repeated until the desired amino acid sequence is synthesized. Finally, the peptide sequence is cleaved from the solid support by trifluoroacetic acid with water, triisopropylsilane and phenol as scavengers, and all the side-chain protecting groups are removed as well. There are several advantages of SPPS.[24] The intermediates can be filtered and washed off, saving a lot of time and labour compared to solution phase synthesis; the coupling reaction can be driven to completion by adding excess reagents during each cycle; the physical losses can be minimized due to the peptides' attachment to the solid support. One disadvantage of SPPS is that a lot of by-products may arise due to incomplete reactions, side reactions or impure reagents.[24] These by-products accumulate on the solid support and contaminate the final products, lowering the overall yield.

(a)   (b)
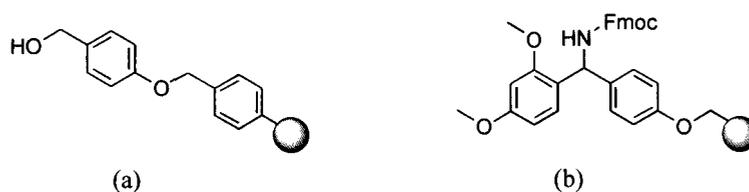
Figure 1.9 (a) Structure of Wang resin, acidolysis to peptide acids. (b) Structure of Rink amide resin, acidolysis to peptide amides.

11
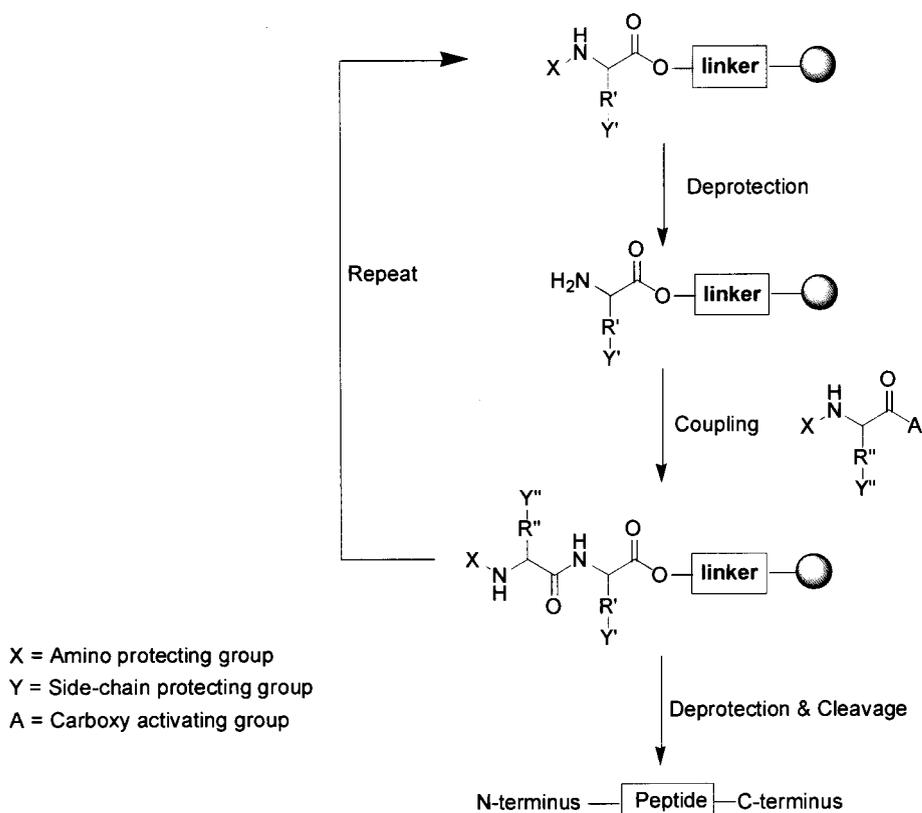
Figure 1.10 The general principle of solid phase peptide synthesis.[24]

1.8 Scope of this Thesis

As a molecular imaging modality, the clinical applications of PET imaging for oncology have been established in the past few years. It has a significant role in the diagnosis, staging, therapy monitoring and assessment of recurrence in cancer.[4] The aim of this thesis is to design orexin peptide analogues and orexin receptor antagonists as potential PET imaging probes for the diagnosis of disease, such as colon cancer which is the third most commonly diagnosed cancer in the world.

Orexin receptor 1 (OX_1R) and orexin receptor 2 (OX_2R) are G-protein coupled receptors

(GPCRs), which were discovered in 1998.[25,26] As two neuropeptides, orexin A and orexin B are two endogenous ligands of OX_1R and OX_2R, regulating food-intake and sleep-awake cycle.[25] In 2004, it was found that OX_1R is expressed in colon cancer cells but not in normal colon cells. Based on the target of OX_1R, gallium-68 labelled truncated orexin A and orexin B were designed as potential peptide based imaging agents targeting colon cancer cells.

Because of the roles in regulation of food-intake and sleep-awake cycle, orexin receptor antagonists, a series of bioactive organic molecules, were developed in the past decade by pharmaceutical companies. Their high binding affinities to orexin receptors leads to the second research project of designing an orexin receptor antagonist for PET imaging, by incorporating fluorine-18 into the antagonist molecule.

References

(1)   Weissleder, R.; Mahmood, U. *Radiology* **2001**, *219*, 316.

(2)   Lee, S.; Xie, J.; Chen, X. *Biochemistry* **2010**, *49*, 1364.

(3)   Langner, J. http://en.wikipedia.org/wiki/File:PET-MIPS-anim.gif.

(4)   Townsend, D. W. In *Positron Emission Tomography*; Valk, P. E.; Delbeke, D.; Bailey, D. L.; Townsend, D. W.; Maisey, M. N., Ed.; Springer-Verlag: London, 2006.

(5)   Liu, Y.; Liu, G.; Hnatowich, D. J. *Materials* **2010**, *3*, 3204.

(6)   Bartholoma, M. D.; Louie, A. S.; Valliant, J. F.; Zubieta, J. *Chemical Reviews* **2010**, *110*, 2903.

(7)   Fani, M.; André, J. P.; Maecke, H. R. *Contrast Media and Molecular Imaging* **2008**, *3*, 53.

(8)   Lasne, M. C.; Perrio, C.; Rouden, J.; Barré, J.; Roeda, D.; Dolle, F.; Crouzel, C. *Topics in Current Chemistry* **2002**, *22*, 201.

(9)   Guillaume, G; Luxen, A.; Nebeling, B.; Argentini, M.; Clark, J.; Pike, V. W. *Applied Radiation and Isotopes* **1991**, *42*, 749.

(10)   Hamacher, K.; Coenen, H. H.; Stöcklin, G. *Journal of Nuclear Medicine* **1986**, *27*, 235.

(11)   Guhlke, S.; Wester, H. J.; Bruns, C.; Stöcklin, G. *Nuclear Medicine and Biology* **1994**, *21*, 819.

(12)   Guhlke, S.; Coenen, H. H.; Stöcklin, G. *Applied Radiation and Isotopes* **1994**, *45*, 715.

(13)   Okarvi, S. M. *European Journal of Nuclear Medicine* **2001**, *28*, 929.

(14)   Hostetler, E. D.; Edwards, W. B.; Anderson, C. J.; Welch, M. J. *Journal of Labelled Compounds and Radiopharmaceuticals* **1999**, *42*, S720.

(15)   Wester, H. J.; Hamacher, K.; Stöcklin, G. *Nuclear Medicine and Biology* **1996**, *23*, 365.

(16)   Lee, S.; Xie, J.; Chen, X. Y. *Chemical Reviews* **2010**, *110*, 3087.

(17)   Krohn, K. A. *Nuclear Medicine and Biology* **2001**, *28*, 477.

(18)   Reubi, J. C. *Endocrine Reviews* **2003**, *24*, 389.

(19)   Jong, M.; Bakker, W. H.; Krenning, E. P.; Breeman, W. P.; Pluijm, M. E.; Bernard, B. F. et al. *European Journal of Nuclear Medicine* **1997**, *24*, 368.

(20)   Weckbecker, G.; Lewis, I.; Albert, R.; Schmid, H. A.; Hoyer, D.; Bruns, C.

Nature Reviews Drug Discovery **2003**, *2*, 999.

(21)   Kwekkeboom, D. J.; Krenning, E. P. *Seminars in Nuclear Medicine* **2002**, *32*, 84.

(22)   Rufini, V.; Calcagni, M. L.; Baum, R. P. *Seminars in Nuclear Medicine* **2006**, *36*, 228.

(23)   Merrifield, R. B. *Journal of the American Chemical Society* **1963**, *85*, 2149.

(24)   Chan, W. C.; White, P. D. In *Fmoc Solid Phase Peptide Synthesis*; Chan, W. C.; White, P. D., Eds.; Oxford University Press: New York, 2003.

(25)   Sakurai, T.; Amemiya, A.; Ishii, M.; Matsuzaki, I.; Chemelli, R. M.; Tanaka, H.; et al. *Cell* **1998**, *92*, 537.

(26)   Delecea, L.; Kilduff, T. S.; Peyron, C.; Gao, S. B.; Foye, P. E.; Danielson, P. E. et al. *National Academy of Sciences* **1998**, *95*, 322.

Chapter 2 Design of Orexin Peptide Based Imaging Agents

2.1 Introduction

2.1.1 Discovery of Orexin Peptides and Their Receptors

In 1998, orexin A and orexin B were identified as two neuropeptides expressed in the hypothalamus area by two independent groups.[1,2] Orexin A and orexin B are derived from the same prepro-orexin precursor (Figure 2.1), composed of 131 amino acid residues.[2] As shown in Figure 2.1, orexin A has 33 amino acids with the C-terminus amidated and orexin B has 28 amino acids with the C-terminus amidated as well.[2] Orexin A and orexin B are two endogenous ligands of two G-protein-coupled receptors (GPCRs), which are named orexin receptor 1 (OX_1R) and orexin receptor 2 (OX_2R).[2] Orexin A has almost the same binding affinity for both OX_1R and OX_2R, while orexin B has a 10-fold higher affinity for OX_2R than for OX_1R.[2]
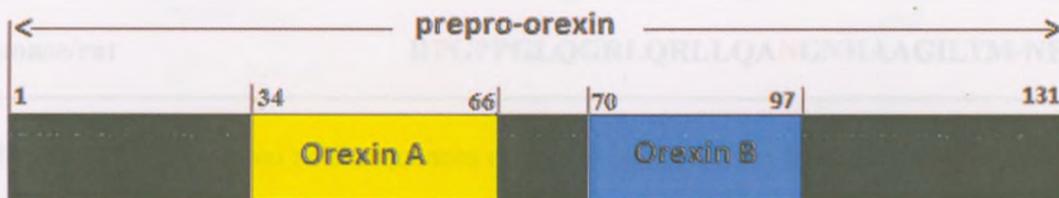
Figure 2.1 The post-translational cleavage of prepro-orexin. Orexin A starts with Gln^{34}, which is presumably transamidated into an N-terminal pyroglutamyl residue by transaminase. The last residue of orexin A is Leu^{66}, which is followed by Gly^{67}. Gly^{67} presumably serves as the $-NH_2$ donor for the C-terminal amidation of orexin A. Orexin B starts with Arg^{70} and ends with Met^{97}, also C-terminally amidated.[2]

2.1.2 Structures of Orexin A and Orexin B

Orexin A has 33 amino acids with two disulfide bonds connecting positions 6 to 12 and 7 to 14. Orexin B has 28 amino acids, with 46% sequence identity with orexin A mainly in the C-terminal region (Figure 2.2). Orexin A is completely conserved in several mammalian species (human, rat, mouse, cow, sheep, dog, and pig). However, human orexin B is slightly different among these mammalian species. For the orexin B in the dog, pig, sheep and cow, serine at position 2 is substituted by proline, whereas mouse and rat orexin B contains proline instead of serine at position 2 and asparagine instead of serine at position 18 (Figure 2.2).[3-5]

```
Orexin A (human/rat/mouse/pig/dog/sheep/cow)


                      EPLPDCCRQKTCSCRLYELLHGAGNHAAGILTL-NH₂
Orexin B

human                 RSGPPGLQGRLQRLLQASGNHAAGILTM-NH₂

pig/dog/sheep/cow     RPGPPGLQGRLQRLLQASGNHAAGILTM-NH₂

mouse/rat             RPGPPGLQGRLQRLLQANGNHAAGILTM-NH₂
```
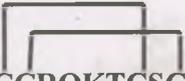
Figure 2.2 The amino acid sequences of orexin A and orexin B in several mammalian species (human, rat, mouse, pig, dog, cow, sheep).

Three independent research groups have studied the secondary structure of orexin A. In 2003, Mark Miskolzie published that orexin A contains two helices spanning the residues Asp^5 to Gln^9 and Leu^{16} to Gly^{22}.[6] However, based on Hai-Young Kim's study published

in 2004, orexin A has two helices, Cys^{14}-His^{21} (Helix I) and Asn^{25}-Leu^{31} (Helix II) (Figure 2.3a).[7] It was also mentioned that the two disulfide bonds make a rigid turn conformation between the Arg^8-Thr^{11} residues. In Tomoyo Takai's publication in 2006, the secondary structure of orexin A was defined as Leu^{16}-Ala^{23} (helix I), Asn^{25}-Thr^{32} (helix II) and Cys^6-Gln^9 (helix III).[8] Similar to orexin A, orexin B has two helices comprised of the residues Leu^7 to Gly^{19} and Ala^{23} to Met^{28}, connected by a flexible loop (Figure 2.3b).[9] All the studies about the secondary structure of orexin A and orexin B have been summarized in Figure 2.4.

(a)   (b)
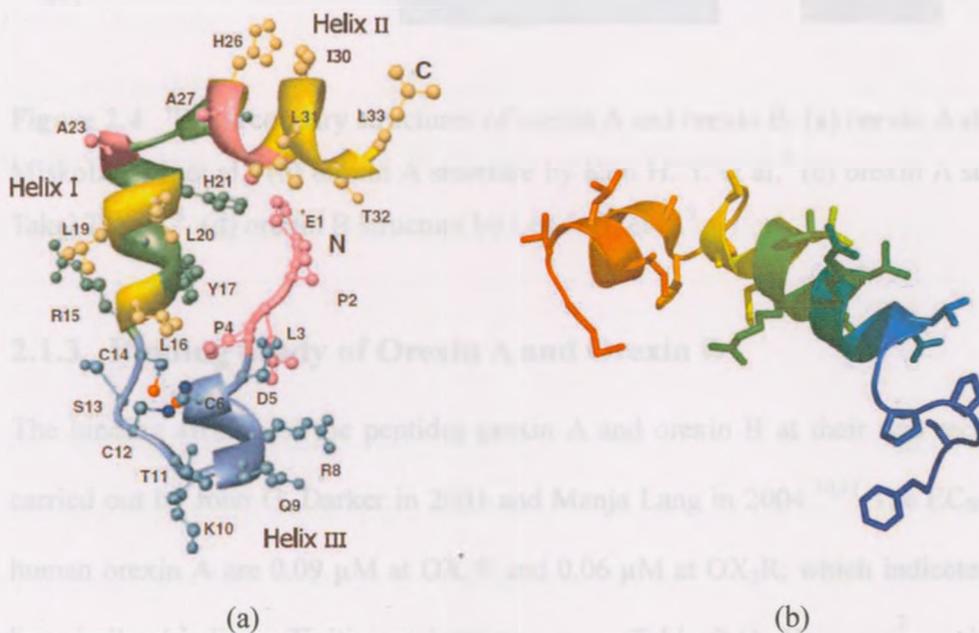
Figure 2.3   (a) The secondary structure of orexin A published by Tomoyo Takai in 2004.[8] (b) The secondary structure of orexin B.[9]

Orexin A (1-33)
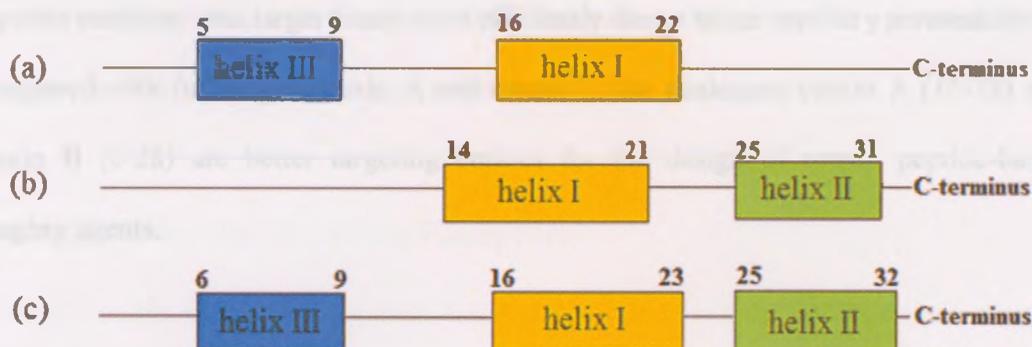
Orexin B (1-28)
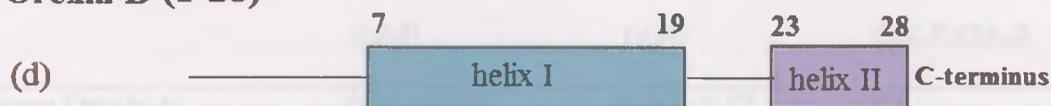
Figure 2.4 The secondary structures of orexin A and orexin B. (a) orexin A structure by Miskolzie M. et al.[6] (b) orexin A structure by Kim H. Y. et al.[7] (c) orexin A structure by Takai T. et al.[8] (d) orexin B structure by Lee J. H. et al.[9]

2.1.3 Binding Study of Orexin A and Orexin B

The binding affinity of the peptides orexin A and orexin B at their two receptors was carried out by John G. Darker in 2001 and Manja Lang in 2004.[10,11] The EC_{50} values of human orexin A are 0.09 µM at OX_1R and 0.06 µM at OX_2R, which indicates orexin A has similar binding affinities at both receptors (Table 2.1). However, orexin B has a higher binding affinity at OX_2R (0.07 µM) than at OX_1R (0.78 µM). Through an N-terminal truncation study, it was identified that the shortest orexin A analogue with a strong agonist effect is orexin A (15-33), while orexin B (6-28) is shortest analogue of orexin B.[10,11] In the design of molecular imaging agents, targeting peptides with low molecular weights are favoured.[12] Small peptides have favourable biodistribution patterns,

such as high uptake by the target and rapid clearance from the body.[12] Also, small peptides penetrate into target tissue more efficiently due to better capillary permeability.[12] Compared with full-length orexin A and orexin B, the analogues orexin A (15-33) and orexin B (6-28) are better targeting entities for the design of orexin peptide-based imaging agents.

Table 2.1 The binding affinities of orexin A, orexin B and their analogues.[11]

Peptides	EC_{50} at OX_1R (μM)	EC_{50} at OX_2R (μM)	Selectivity OX_1R/OX_2R
Human Orexin A	0.09 ± 0.05	0.06 ± 0.02	1.5
Human Orexin B	0.78 ± 0.07	0.07 ± 0.03	11.1
Human Orexin A (15-33)	1.79 ± 0.46	0.42 ± 0.08	4.3
Human Orexin B (6-28)	0.73 ± 0.04	0.13 ± 0.06	5.6

The effect of a single amino acid residue on binding activities was investigated by the L-alanine scan.[10,11] The replacement of a single amino acid by L-alanine led to a great loss of the activity at both receptors for the amino acids Leu[16], Leu[19], Leu[20], His[26], Gly[29], Ile[30], Leu[31], Thr[32] and Leu[33] in orexin A (15-33). When Leu[15], Gly[24], Ile[25], Leu[26], Thr[27] in orexin B (6-28) were displaced by L-alanine, the EC_{50} values were above 1000 μM, incapable of activating orexin receptors. Based on the results from the L-alanine scan study, it was discovered that most critical amino acids for binding activities are located in C-terminus, and thus the C-terminal of orexin A (15-33) and orexin B (6-28) are much

more significant for binding activities than the N-terminal. Therefore, when designing orexin imaging agents, the imaging label should be attached to the orexin peptides through the N-terminus rather than C-terminus.

2.1.4   Distribution of Orexin Receptors

As mentioned in section 2.1.1, orexin A and orexin B bind to two GPCRs, orexin receptor 1 (OX_1R) and orexin receptor 2 (OX_2R).[2] The human OX_1R is a protein with 425 amino acids and seven putative transmembrane helices. The human OX_2R is a 444-amino-acid protein with seven putative transmembrane helices as well. OX_2R shares 64% amino acid identity with OX_1R. They were originally identified in the region of brain, but later studies show that they are also expressed in peripheral tissues, such as kidney, intestine and pancreas (Table 2.2).[2,13-17]

Studies of the expression of OX_1R and OX_2R in peripheral tissues established the roles of orexins in regulating intestinal motility and insulin release, controlling pancreatic hormone secretion and glucose metabolism.[18] In normal pancreas, OX_1R-positve cells are mainly present in the peripheral parts of the islet, while the number and distribution of OX_1R-positive cells are both changed in the diabetic pancreas.[19] After the onset of diabetes, OX_1R-positive cells distribute in both peripheral and central regions of islets, and the number of OX_1R-positive cells increases significantly, from 20% to 60% of the total pancreatic islet cells compared with normal pancreas.[19] The differences in the distribution regions and the number of OX_1R-positive cells may lead to the development of orexin based imaging agents for the analysis of the functioning of pancreas.

Table 2.2 The expression of orexin receptors in rat tissues.

Rat tissue	OX_1R	OX_2R	Rat tissue	OX_1R	OX_2R
Brain	+	+	Stomach	–	–
Pituitary	+	+	Pancreas	+	+
Adrenal	+	+	Liver	–	–
Gonads	+	–	Spleen	–	–
Kidney	+	–	Heart	–	–
Small intestine	+	+	Lung	–	+
Skeletal muscle	–	–	Thyroid	+	–

+, detected; -, absent

2.1.5 Expression of Orexin Receptor 1 in Colon Cancer Cells

In 2004, it was published that OX_1R was expressed in colon cancer cells, but it was not present in normal colonic epithelial cells.[20] The expression of OX_1R was verified in the following colon cancer cell lines: Caco2, SW480, LoVo and HT-29. There is one exception, the HCT 116 colon cancer line, in which no expression of OX_1R was observed. Later research conducted by Voison T. et al. demonstrated that OX_1R was expressed in other colon cancer cell lines as well: HT29-FU, SW620, Colo205, T84, TS174T and SW48 (Figure 2.5).[21] The LoVo cell line has the highest expression of OX_1R. In Voison's research, all the thirty-eight colon tumor specimens tested were immunoreactive for OX_1R. The mean percentage of immunoreactive cells was around 80% (Figure 2.6). Based on the expression of OX_1R in colon cancer cells, it may be feasible to design orexin based imaging agents targeting colon cancer cells.
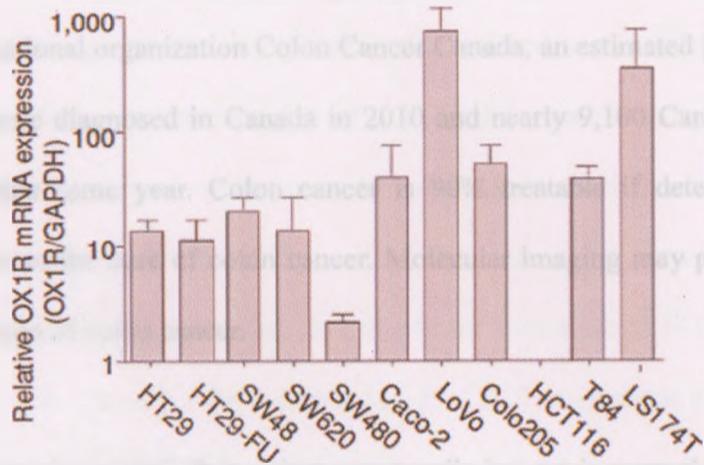
Figure 2.5 Relative OX$_1$R mRNA expression in colon cell lines. LoVo has the highest expression of OX$_1$R; SW480 has the lowest expression of OX$_1$R; HCT116 doesn't express OX$_1$R. [21]
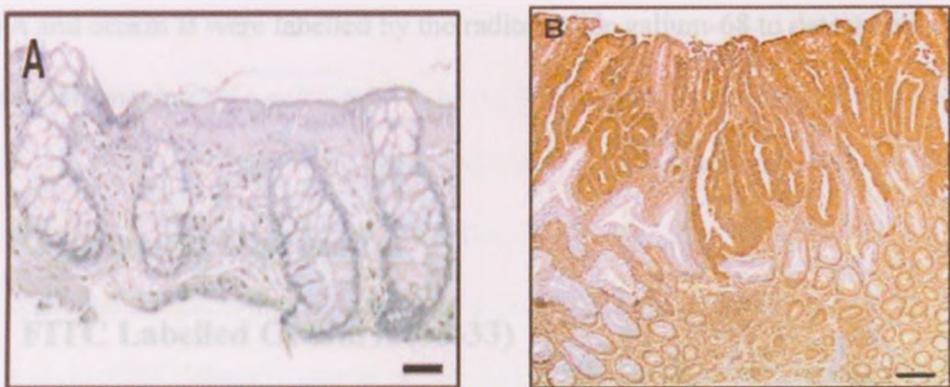
Figure 2.6 A. Paraformaldehyde-fixed sigmoid from a patient with irritable bowel. No immunoreactive signal was observed. B. Paraformaldehyde-fixed colon tumors in sigmoid showed immunoreactivity OX$_1$R, indicated by the brown area.[21]

2.2 Objective

23

Colon cancer is the third most commonly diagnosed cancer in the world. Based on the data from the national organization Colon Cancer Canada, an estimated 22,500 new colon cancer cases were diagnosed in Canada in 2010 and nearly 9,100 Canadians died from colon cancer that same year. Colon cancer is 90% treatable if detected early. Early detection is key to the cure of colon cancer. Molecular imaging may provide a way for the early detection of colon cancer.

Due to the expression of OX_1R in colon cancer cells but not in normal colonic epithelial cells, orexin A and orexin B have great potential to be designed as molecular imaging probes targeting colon cancer cells. In order to evaluate the targeting ability in cells, orexin A and orexin B were labelled by fluorescein isothiocyanate (FITC) to test whether they were uptaken by colon cancer cells. In order to evaluate the ability to target *in vivo*, orexin A and orexin B were labelled by the radionuclide galium-68 to detect colon cancer cells via PET imaging.

2.3 Results and Discussion

2.3.1 FITC Labelled Orexin A (15-33)

Orexin A (15-33) was made by solid phase peptide synthesis (SPPS) with Rink-amide resin and Fmoc-protected amino acids starting from the C-terminus of orexin A (15-33). *N*-Fmoc was removed by 20% piperidine in dimethylformamide (DMF). Amino acids were activated by 1-[bis(dimethylamino)methylene]-1H-benzotriazolium hexafluorophosphate 3-oxide (HBTU) in the presence of *N,N*-diisopropylethylamine (DIPEA). After the synthesis of the peptide sequence, a linker amino hexanoic acid (Ahx)

was coupled to the N-terminus of orexin A (15-33) to reduce the effects of the label on the biological binding activities. Then FITC was attached to the linker by the reaction between the isothiocyanate functionality of FITC and the amino group of the linker. At the end, peptide was cleaved off the resin by the cocktail of trifluoroacetic acid (TFA), water (H_2O), triisopropylsilane (TIS) and phenol. Under these conditions, all the protecting groups were also removed, resulting in the formation of FITC-labelled orexin A (15-33), that is fluorescein-Ahx-orexin A (15-33) (**1**). The synthetic procedure of FITC labelled orexin A (15-33) is shown in Scheme 2.1.

It was found that FITC-labelled orexin A (15-33) was difficult to dissolve in H_2O. The solubility issue might be caused by the following two reasons. First of all, orexin A (15-33) is a long peptide with 19 amino acids and complex structures. More than half of those 19 amino acids are hydrophobic. Second, FITC hardly dissolves in H_2O, contributing to the poor solubility of FITC-labelled orexin A (15-33). In order to improve the solubility of orexin A (15-33), the short PEG chain [2-[2-amino ethoxy] ethoxy] acetic acid (AEEA) was used as the linker instead of Ahx. Compared with Ahx linker, AEEA is more hydrophilic and might improve the water solubility of the peptide. When AEEA was introduced to FITC-labelled orexin A (15-33), the imaging agent fluorescein-AEEA-orexin A (15-33) (**2**) was made. The solubility of **2** was slightly improved compared to **1**.
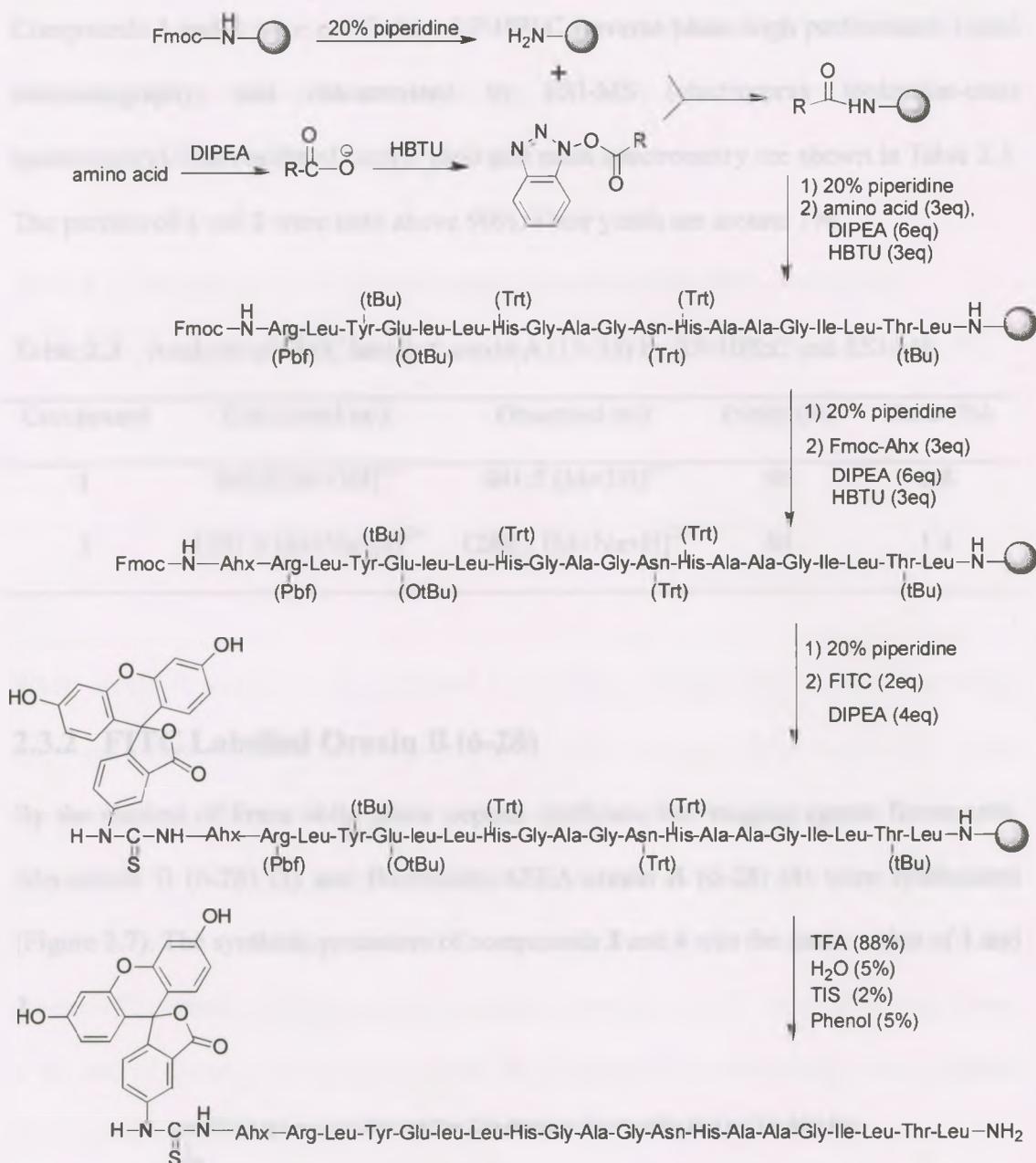
Scheme 2.1 Synthetic procedure of FITC labelled orexin A (15-33) with Ahx as the linker via Fmoc solid phase peptide synthesis. Grey circles represent the solid support, Rink-amide resin.

Compounds **1** and **2** were purified by RP-HPLC (reverse phase-high performance liquid chromatography) and characterized by ESI-MS (electrospray ionization-mass spectrometry). The results of purity, yield and mass spectrometry are shown in Table 2.3. The purities of **1** and **2** were both above 90%. Their yields are around 1%.

Table 2.3 Analysis of FITC labelled orexin A (15-33) by RP-HPLC and ESI-MS.

Compound	Calculated m/z	Observed m/z	Purity (%)	Yield (%)
1	840.8 [M+3H]$^{2+}$	841.5 [M+3H]$^{2+}$	98	0.8
2	1287.6 [M+Na+H]$^{2+}$	1288.1 [M+Na+H]$^{2+}$	94	1.4

2.3.2   FITC Labelled Orexin B (6-28)

By the method of Fmoc solid phase peptide synthesis, the imaging agents fluorescein-Ahx-orexin B (6-28) (**3**) and fluorescein-AEEA-orexin B (6-28) (**4**) were synthesized (Figure 2.7). The synthetic procedure of compounds **3** and **4** was the same as that of **1** and **2**.
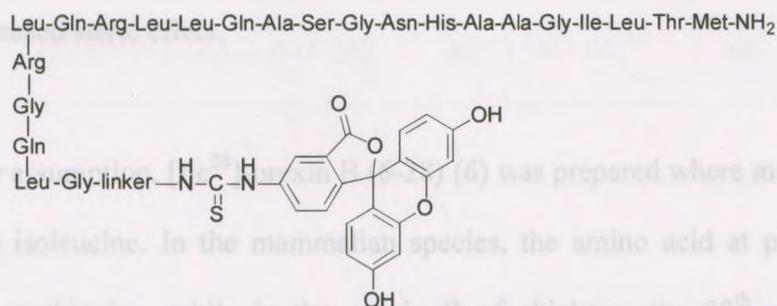
Figure 2.7   Structures of fluorescein-Ahx-orexin B (6-28) (**3**) and fluorescein-AEEA-orexin B (6-28) (**4**). The linker represents Ahx for **3** and AEEA for **4**.

Compounds **3** and **4** were purified by RP-HPLC and characterized by ESI-MS. The results of purity, yield and mass spectrometry are shown in Table 2.4. The purities of **3** and **4** were both above 90%. Their yields are around 1%.

Table 2.4 Analysis of FITC labelled orexin B (6-28) by RP-HPLC and ESI-MS.

Compound	Calculated m/z	Observed m/z	Purity (%)	Yield (%)
3	1453.7 [M+2H]$^{2+}$	1454.2 [M+2H]$^{2+}$	98	1.5
4	1469.7 [M+2H]$^{2+}$	1470.2 [M+2H]$^{2+}$	93	1.0

When orexin B (6-28) (**5**) was analyzed by LC-MS, it always had an impurity, whose mass was around 16 above the exact mass of **5**. The C-terminus of **5** is methionine, which can undergo alkylation and oxidation. The cocktail used for the cleavage of **5** from the resin was TFA, TIS, H_2O and phenol (88:2:5:5). The scavengers were enough to prevent the alkylation of methionine. Thus, it was assumed that Met^{28} was oxidized during the process of synthesis resulting in the by-product with a mass of 16 above. Also, Met^{28} was at the end of C-terminus, which increased the possibilities for methionine to be oxidized due to a decreased steric effect.

To verify our assumption, [Ile^{28}]-orexin B (6-28) (**6**) was prepared where methionine was displaced by isoleucine. In the mammalian species, the amino acid at position 28 of orexin B is methionine, while in the orexin B of chickens, the 28th amino acid is isoleucine (Figure 2.8).[3] Because of the similar structures of methionine and isoleucine, it

was expected that the binding affinity of **5** to the receptors would remain satisfactory after the methionine was displaced by isoleucine.

Orexin B (6-28)

human   **GLQGRLQRLLQASGNHAAGILTM-NH₂**

chicken   **GLQGRLQRLLQASGNHAAGILTI-NH₂**

Figure 2.8   The amino acid sequences of human orexin B (6-28) and chicken orexin B (6-28).

As assumed, after methionine was displaced by isoleucine, compound **6** did not have an impurity with the mass of 16 above, which was supported by the data obtained from LC-MS as shown in Figure 2.9 and Table 2.5. Based on the data from ESI-MS, the mass difference between **5** and [Met(O)²⁸]-orexin B (6-28) (**7**) was 15.96.

Table 2.5   The ESI-MS data of compounds **6**, **7** and **8**.

Compound	Peptide	Calculated m/z	Observed m/z
5	Orexin B (6-28)	801.8 $[M+3H]^{3+}$	804.5 $[M+3H]^{3+}$
6	[Ile²⁸]-orexin B (6-28)	795.8 $[M+3H]^{3+}$	798.5 $[M+3H]^{3+}$
7	[Met(O)²⁸]-orexin B (6-28)	807.1 $[M+3H]^{3+}$	809.8 $[M+3H]^{3+}$
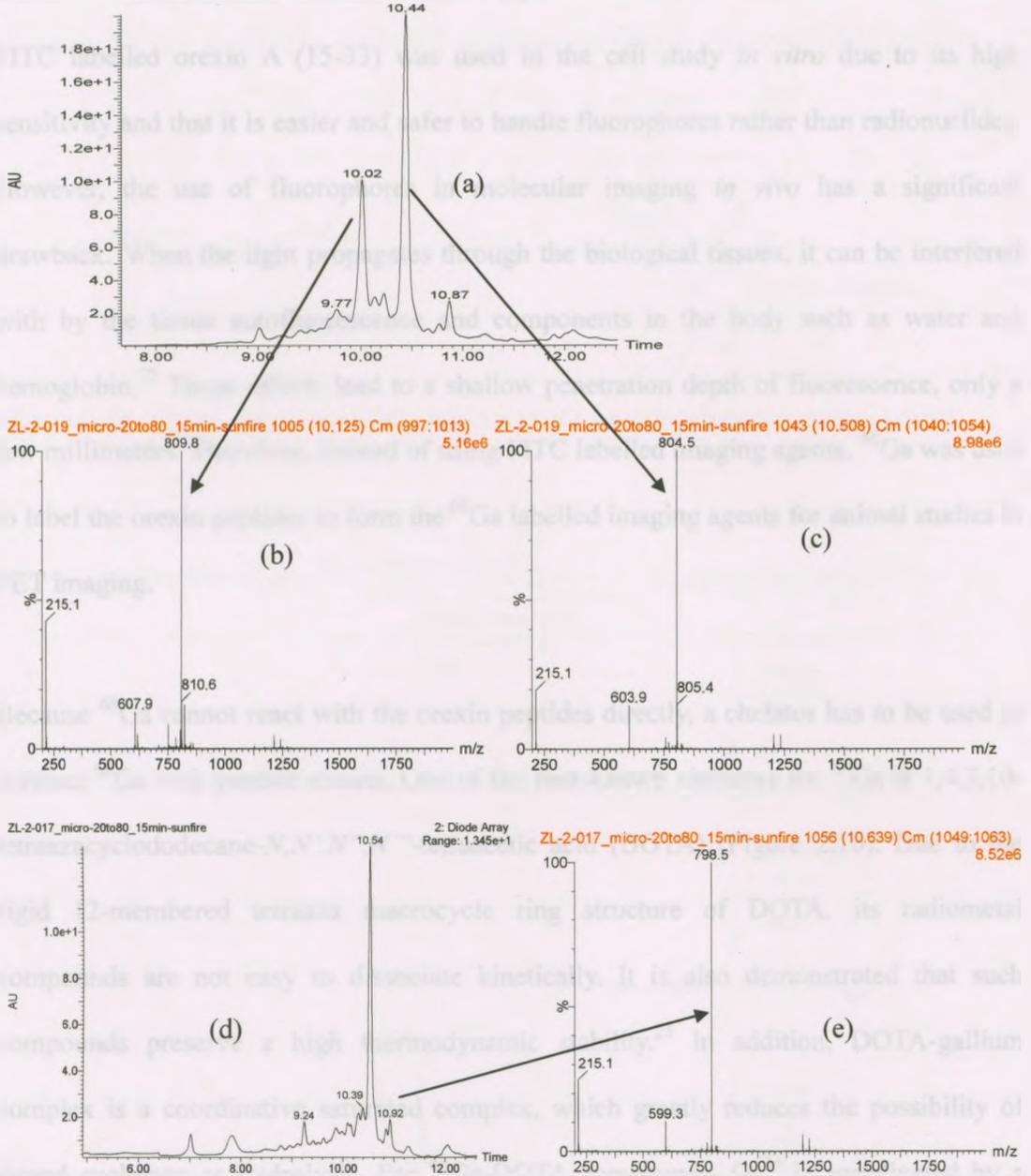
Figure 2.9 (a) HPLC UV chromatogram of crude reaction mixture **5** (RT = 10.44) and **7** (RT = 10.02); (b) Mass spectrum of **7**, m/z : 809.8 [M+3H]³⁺; (c) Mass spectrum of **5**, m/z : 804.5 [M+3H]³⁺; (d) HPLC UV chromatogram of crude reaction mixture **6** (RT = 10.44); (e) Mass spectrum of **6**, m/z : 798.5 [M+3H]³⁺.

2.3.3 ^{68}Ga Labelled Orexin A (15-33)

FITC labelled orexin A (15-33) was used in the cell study *in vitro* due to its high sensitivity and that it is easier and safer to handle fluorophores rather than radionuclides. However, the use of fluorophores in molecular imaging *in vivo* has a significant drawback. When the light propagates through the biological tissues, it can be interfered with by the tissue autofluorescence and components in the body such as water and hemoglobin.[22] Those effects lead to a shallow penetration depth of fluorescence, only a few millimeters. Therefore, instead of using FITC labelled imaging agents, ^{68}Ga was used to label the orexin peptides to form the ^{68}Ga labelled imaging agents for animal studies in PET imaging.

Because ^{68}Ga cannot react with the orexin peptides directly, a chelator has to be used to connect ^{68}Ga with peptide chains. One of the best-known chelators for ^{68}Ga is 1,4,7,10-tetraazacyclododecane-*N,N',N'',N'''*-tetraacetic acid (DOTA) (Figure 2.10). Due to the rigid 12-membered tetraaza macrocycle ring structure of DOTA, its radiometal compounds are not easy to dissociate kinetically. It is also demonstrated that such compounds preserve a high thermodynamic stability.[23] In addition, DOTA-gallium complex is a coordinative saturated complex, which greatly reduces the possibility of ligand exchange or hydrolysis. For ^{68}Ga-DOTA compounds, Ga^{3+} is coordinated by a N_4O_2 donor set to form a cis-pseudooctahedral coordination structure. Besides the two carboxylic acid groups contributing to the gallium coordination, another carboxylic acid is conjugated to the amino acid of the peptide (Figure 2.10).[24] Due to the advantages of ^{68}Ga labelled DOTA-conjugates, the imaging agent ^{68}Ga-DOTA-orexin A (15-33) (**8**) was

designed. The synthetic procedure of DOTA-orexin A (15-33) (**9**) is shown in Scheme 2.2. Compound **9** was purified by RP-HPLC and characterized by ESI-MS (Table 2.6).
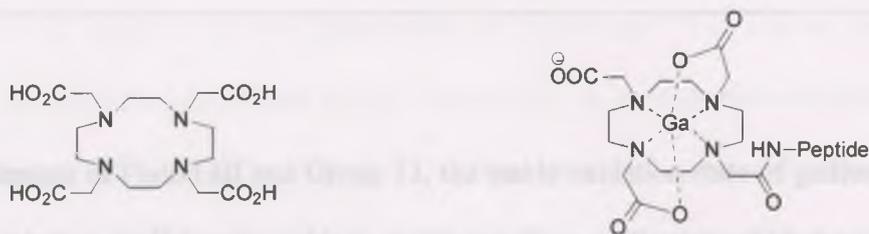
Figure 2.10 The structures of DOTA (left) and DOTA-peptide labelled by gallium (right).
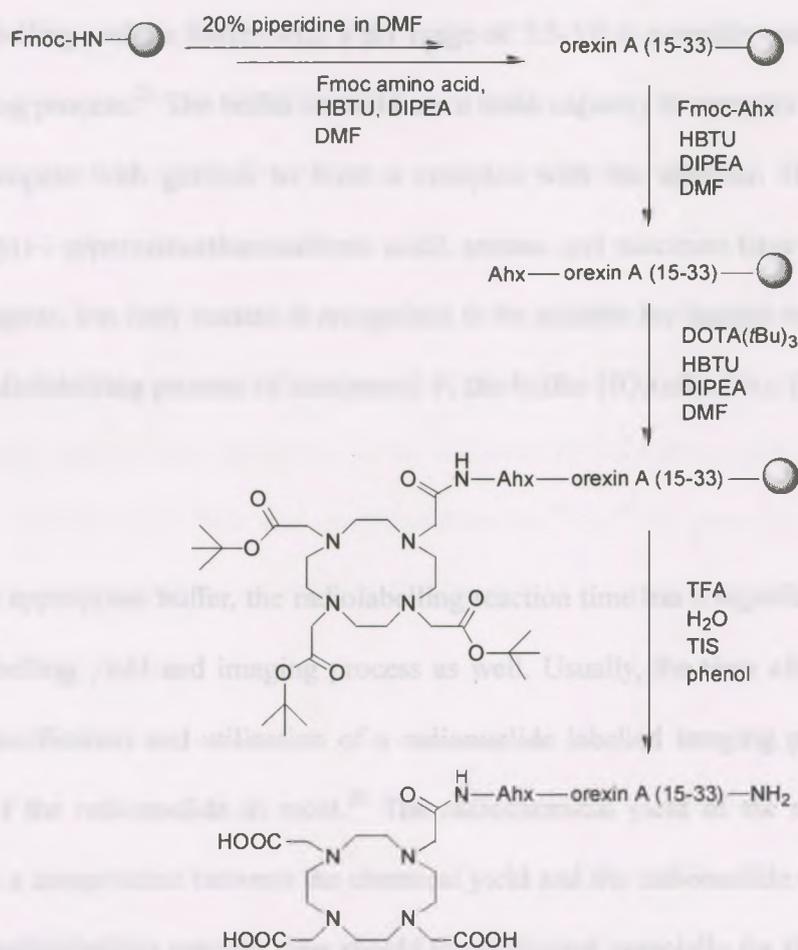
Scheme 2.2 Synthetic procedure for the preparation of **9**.

Table 2.6 Analysis of synthesized DOTA-orexin A (15-33) (9).

Compound	Calculated m/z	Observed m/z	Purity (%)	Yield (%)
9	1270.2 [M+Na+H]$^{2+}$	1270.7 [M+Na+H]$^{2+}$	98	5.2

As the element of Period Ш and Group 13, the stable oxidation state of gallium is +3 in aqueous solution. Ga^{3+} is only stable in acidic conditions. When the pH is between 3 and 7, insoluble $Ga(OH)_3$ is formed without stabilizing ligands. In basic conditions, $Ga(OH)_3$ re-dissolves into $[Ga(OH)_4]^-$. In order to avoid the hydrolysis of gallium and maximize the radiolabelling yield, a buffer with a pH range of 3.5-5.0 is normally used during the radiolabelling process.[25] The buffer should have a weak capacity to complex with gallium and not compete with gallium to form a complex with the chelator. HEPES (4-(2-hydroxyethyl)-1-piperazineethanesulfonic acid), acetate, and succinate have been used as buffering agents, but only acetate is recognized to be suitable for human use.[25] Thus, in the ^{68}Ga radiolabelling process of compound **9**, the buffer HOAc/NaOAc (PH~5.0) was used.

Besides the appropriate buffer, the radiolabelling reaction time has a significant effect on the radiolabelling yield and imaging process as well. Usually, the time allowed for the synthesis, purification and utilization of a radionuclide labelled imaging probe is three half-lives of the radionuclide at most.[26] The radiochemical yield of the radiolabelling synthesis is a compromise between the chemical yield and the radionuclide decay.[27] As a result, the radiolabelling reaction time should be minimized especially for the short-lived

radionuclides such as ^{68}Ga and heating provides a way to accelerate the radiolabelling reaction. Moreover, the radiolabelling kinetics of DOTA-bioconjugates is slow, which results in a very low radiolabelling yield at room temperature.[28] Thus, elevated reaction temperature is required for the coordination of DOTA and [68]Ga. On the other hand, peptides are liable to degradation at high temperature, so a temperature-dependent study was carried out before labelling **9** with [68]Ga. The solution of compound **9** was heated at 50°C, 70°C, 80°C, 90°C and 100°C for 20 minutes at each temperature, following by LC-MS analysis. Over this temperature range, there was no peptide degradation observed.

The reaction time was studied at 70°C through the reaction between **9** and non-radioactive gallium nitrate in the HOAc / NaOAc buffer. The reaction was followed up by LC-MS at 5-minute intervals. The labelling reaction was complete within 10 minutes.

Based on the results from the studies of reaction buffer, reaction temperature and reaction time, the conditions for the radiolabelling of compound **9** with ^{68}Ga were determined. The radiolabelling reaction was carried out in the NaOAc / HOAc buffer (pH~5) at 70°C for 20 minutes (Scheme 2.3). [68]Ga was produced from the [68]Ge/^{68}Ga generator and the final radiolabelled **9** was analyzed by RP-HPLC (Figure 2.11). The radiochemical yield of **8** was 22%.

34
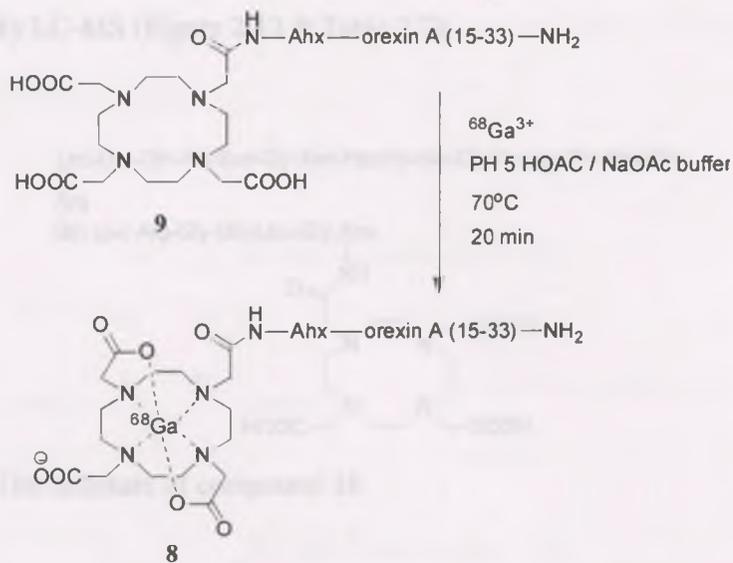
Scheme 2.3   Gallium-68 radiolabelling of compound 9.
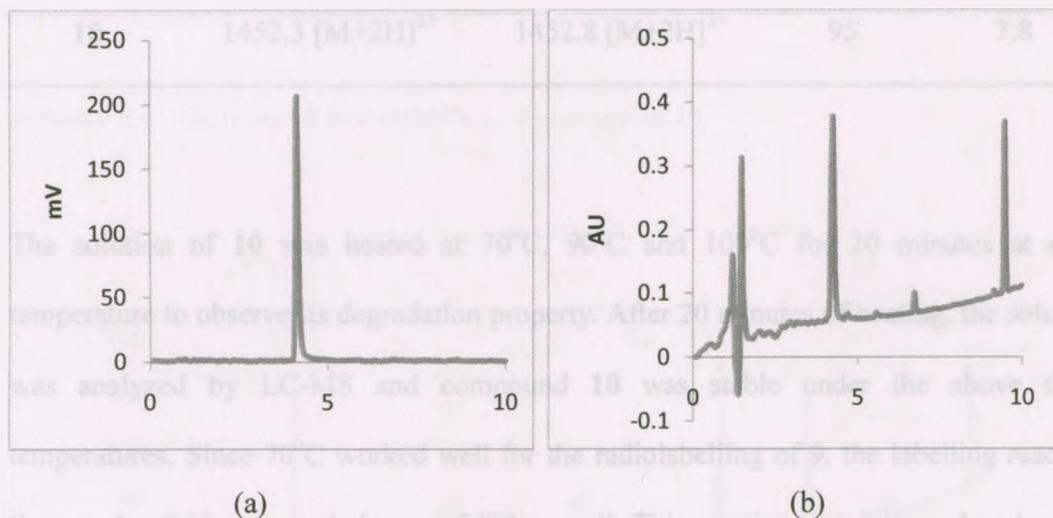
Figure 2.11 (a) The HPLC radiochromatogram of compound **8**. (b) The HPLC UV chromatogram of the reaction mixture from ^{68}Ga radiolabelling.

2.3.4 ^{68}Ga Labelled Orexin B (6-28)

Using the same synthetic procedure as DOTA-orexin A (15-33) (**9**), DOTA-Ahx-orexin B (6-28) (**10**) was synthesized by the method of SPPS. Compound **10** was purified and

characterized by LC-MS (Figure 2.12 & Table 2.7).
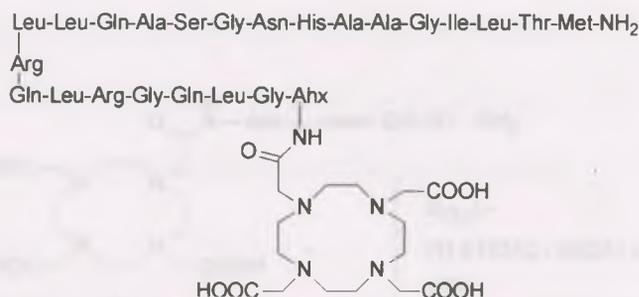
Figure 2.12   The structure of compound 10.

Table 2.7   Analysis of synthesized DOTA-Ahx-orexin B (6-28) (10).

Compound	Calculated m/z	Observed m/z	Purity (%)	Yield (%)
10	1452.3 $[M+2H]^{2+}$	1452.8 $[M+2H]^{2+}$	95	7.8

The solution of 10 was heated at 70°C, 90°C and 100°C for 20 minutes at each temperature to observe its degradation property. After 20 minutes of heating, the solution was analyzed by LC-MS and compound 10 was stable under the above three temperatures. Since 70°C worked well for the radiolabelling of 9, the labelling reaction time study of 10 was carried out at 70°C as well. This reaction was followed up by LC-MS every 5 minutes over 25 minutes. However, the reaction was not complete after 25 minutes. In order to minimize the reaction time, the temperature was elevated to 90°C and the reaction was complete within 15 minutes. As a result, the radiolabelling of 10 was carried out in the HOAc / NaOAc buffer (pH~5) at 90°C for 20 minutes (Scheme 2.4). ^{68}Ga was produced from the ^{68}Ge/^{68}Ga generator and the final ^{68}Ga labelled 10 was

analyzed by RP-HPLC (Figure 2.13). The radiochemical yield of [^{68}Ga]-DOTA-Ahx-Orexin B (6-28) (11) was 85%.

O═N—Ahx—orexin B(6-28)—NH$_2$

HOOC

HOOC—COOH

10

^{68}Ga^{3+}
PH 5 HOAC / NaOAc buffer
90°C
20 min

O═N—Ahx—orexin B (6-28)—NH$_2$

^{68}Ga

OOC

11
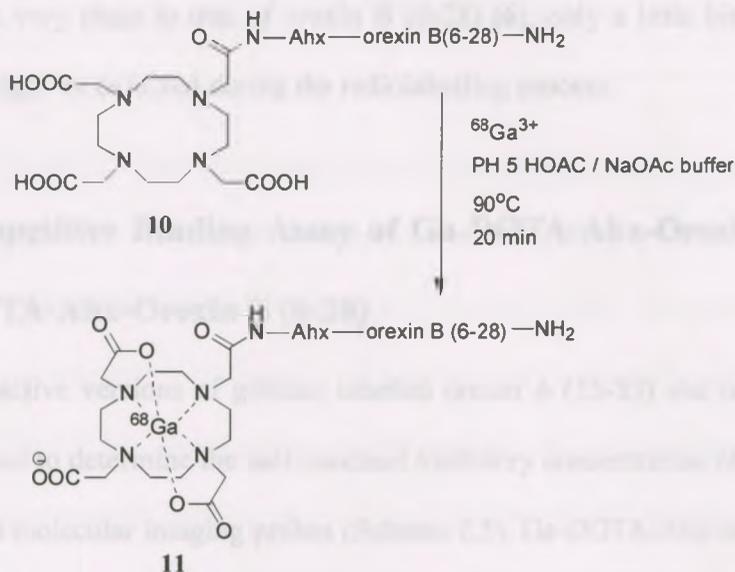
Scheme 2.4 Gallium-68 radiolabelling of compound **10**.

(a)   (b)
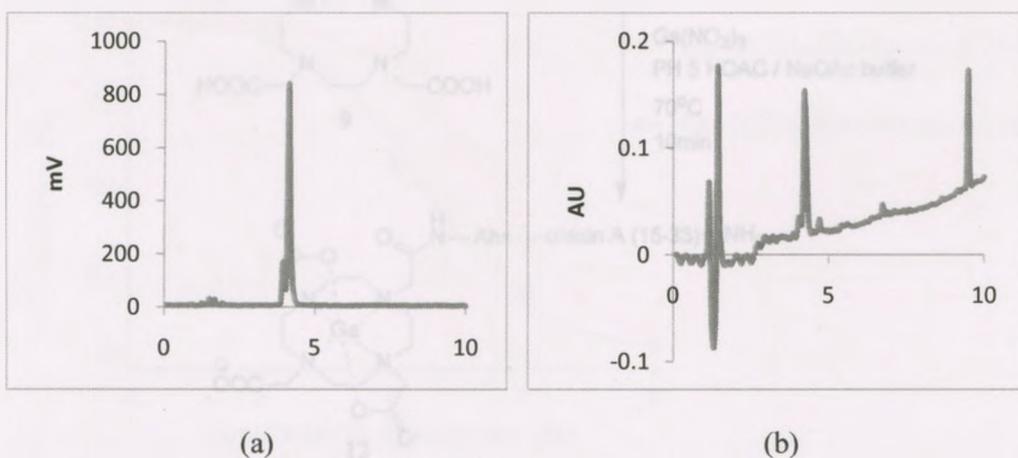
Figure 2.13 (a) The HPLC radiochromatogram of compound **11**. (b) The HPLC UV chromatogram of the reaction mixture from ^{68}Ga radiolabelling.

As shown in the two chromatograms in Figure 2.13, there was a tiny peak before the major peak between the retention time of 4 min and 5 min. As mentioned in section 2.3.2, the Met[28] of orexin B (6-28) could be oxidized. The retention time of [Met(O)[28]]-orexin B (6-28) (7) was very close to that of orexin B (6-28) (6), only a little bit shorter. Thus, compound 9 might be oxidized during the radiolabelling process.

2.3.5   Competitive Binding Assay of Ga-DOTA-Ahx-Orexin A (15-33) and Ga-DOTA-Ahx-Orexin B (6-28)

The non-radioactive versions of gallium labelled orexin A (15-33) and orexin B (6-28) were synthesized to determine the half maximal inhibitory concentration (IC$_{50}$) of orexin-based potential molecular imaging probes (Scheme 2.5). Ga-DOTA-Ahx-orexin A (15-33) (12) and Ga-DOTA-Ahx-orexin B (6-28) (13) was analyzed by RP-HPLC and characterized by ESI-MS. The results are shown in Table 2.8.
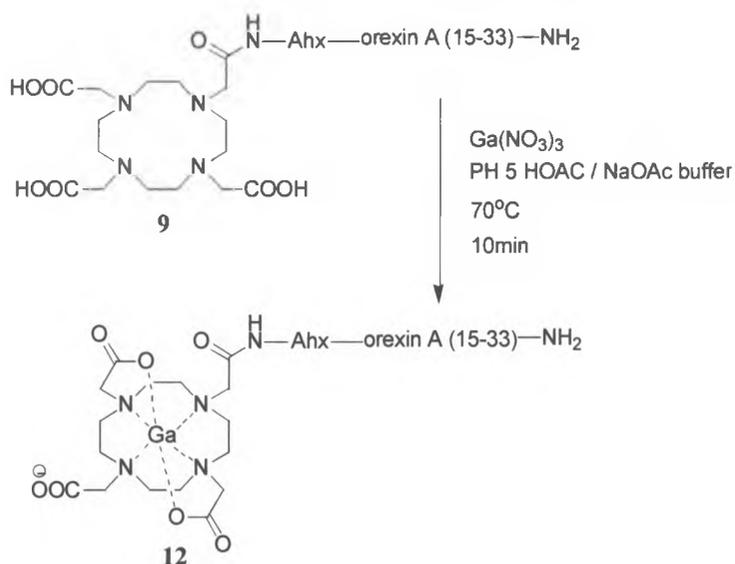
Scheme 2.5   The gallium labelling of compound 9 to give Ga-DOTA-Ahx-orexin A (15-33) (12)

38

Table 2.8 Analysis of compounds **12** and **13** by RP-HPLC and ESI-MS.

Compound	Calculated m/z	Observed m/z	Purity (%)
12	1293.2 $[M+2H]^{2+}$	1293.2 $[M+2H]^{2+}$	95
13	1508.2 $[M+2Na]^{2+}$	1508.7 $[M+2Na]^{2+}$	98

The IC_{50}s of **12** and **13** were determined by the competitive radioligand binding assay using chinese hamster ovary (CHO) cells expressing OX_1R, through a commercial Pharmacology company Ricerca Biosciences (Concord, Ohio). Receptor binding was measured by the competitive binding of $[^{125}I]$-orexin A with increasing concentrations of **12** and **13** (10^{-5} to 10^{-9} M). Based on the response curves, the concentration of **12** required to displace 50% of specific radioligand binding (IC_{50}) was 629 nM and the IC_{50} of **13** was 168 nM (Figure 2.14). As expected, their IC_{50}s were lower than those of orexin A and orexin B, but they were still promising for the design of molecular imaging probes.
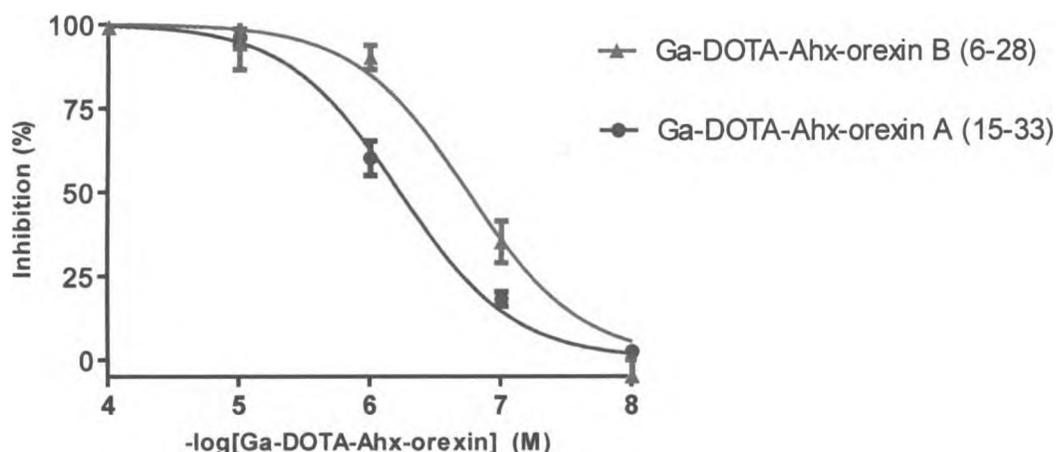
Figure 2.14 Competitive binding of Ga-DOTA-Ahx-orexin A (15-33) **(12)** and Ga-DOTA-Ahx-orexin B (6-28) **(13)** versus $[^{125}I]$-orexin A on CHO/OX_1R cells.

2.4 Conclusion

This project aims to design orexin analogues as potential imaging probes targeting colon cancer cells in PET imaging. The orexin A (15-33) and orexin B (6-28) peptide sequences were labelled with FITC and gallium-68 successfully. The radiochemical yield of $[^{68}Ga]$-DOTA-Ahx-Orexin B (6-28) (8) was low at $70^{o}C$ in the pH 5 HOAc / NaOAc buffer. To increase the radiochemical yield, the temperature can be elevated and the pH of the buffer can be optimized.

The $IC_{50}s$ of Ga-DOTA-Ahx-orexin A (15-33) (12) and Ga-DOTA-Ahx-orexin B (6-28) (13) were determined as well. Compound 13 has a much higher binding affinity at OX_1R than 12. Based on the binding affinity, compound 13 is the leading candidate for a PET imaging agent targeting orexin receptors. Besides, orexin B (6-28) is more water soluble than orexin A (15-33). It is easier to purify orexin B (6-28) than orexin A (15-33). However, orexin B (6-28) has a drawback as it may be oxidized during the synthetic process and radiolabelling process. This drawback may be avoided by a further modification: displacing the methionine at position 28 with another amino acid which does not significantly affect the binding affinities of orexin B (6-28).

2.5 Experimental

All peptides were synthesized manually or by using an APEX396 peptide synthesizer obtained from AAPPTec in Louisville with the method of solid phase peptide synthesis and purified by Waters FractionLynx autopurification RP-HPLC system obtained from Waters Corporation in Milford. The solvents were purchased from VWR, Fisher

Scientific, or Sigma Aldrich and used without further purification. The Rink-amide resin, standard Fmoc amino acids, Fmoc-aminohexanoic acid (Ahx), HBTU coupling reagents were provided by Peptides International in Louisville. DOTA-tris-(*t*Bu)-ester was obtained from CheMatech in Dijon. The linker [2-[2-amino ethoxy] ethoxy] acetic acid (AEEA) was synthesized and purified in our laboratory as described in Chapter 3. The purity of Fmoc-AEEA linker was 97% as analyzed by HPLC.

2.5.1   Synthesis of FITC Labelled Orexin A Analogue (1 & 2)

Rink amide MBHA resin (0.1 mmol) was swelled in 2 mL dichloromethane (DCM) for 2 minutes, repeated 3 times and then in 2 mL *N,N*-dimethylformamide (DMF) once. Fmoc deprotection of Rink amide MBHA resin was performed by agitation in a solution of 20% piperidine in DMF twice, 5 minutes for the first time and then 15 minutes for the second time. After the first deprotection, the resin was washed by 2 mL DMF (3 times). After the second deprotection, the resin was washed by 2 mL DMF (3 times), DCM (3 times) and DMF (3 times). Amino acid (0.3 mmol) was dissolved in 2 mL DMF and activated by 1-[bis(dimethylamino)methylene]-1H-benzotriazolium hexafluorophosphate 3-oxide (HBTU) (0.3 mmol) in the presence of *N,N*-diisopropylethylamine (DIPEA). The coupling step was done twice for each amino acid, 45 minutes for the first time and 120 minutes for the second time. The resin was washed by 2 mL DMF (3 times) after each coupling step. Fmoc-aminohexanoic acid (Ahx) or [2-[2-(Fmoc-amino) ethoxy] ethoxy] acetic acid (AEEA) was coupled to the N-terminus of peptides using the same deprotection and coupling conditions described above. Then fluorescein isothiocyanate FITC (0.4 mmol) dissolved in 2 mL DMF with DIPEA was added into the resin, shaking

for 4 hours.

The full cleavage of peptides was performed in a solution of trifluoroacetic acid (TFA), water (H_2O), triisopropylsilane (TIS) and phenol (88:5:2:5) for 12 hours. After being treated in the cleavage cocktail solutions, the resin was removed by filtration and washed with TFA twice. All the filtrates were combined and cold tert-butyl methyl ether (TBME) was added into the filtrates. The mixture was cooled down on ice while waiting for the precipitation of peptides (10 minutes) and then centrifuged at 3000 rpm for 10 minutes at $-10^{\circ}C$. This step was repeated twice, and then the precipitate was dissolved in water, frozen in dry ice and dried on a lyophilizer yielding solid yellow powders **1** or **2**.

The peptides were analyzed and purified by RP-HPLC/ESI-MS. This RP-HPLC system was equipped with a Waters 600 controller, Waters Prep degasser, and Waters MassLynx software (version 4.1). The mobile phases were 0.1% TFA in H_2O (solvent A) and 0.1% TFA in CH_3CN (solvent B). The linear flow rates of the gradients were 1.5 mL/min and 20 mL/min for analytical and preparative RP-HPLC. The eluate was monitored by a Waters 2998 Photodiode array detector. During purification, the fractions were collected and then lyophilized to become powders and subsequently analyzed by ESI/MS (Waters Micromass Quattro Micro™ API).

During the peptide synthesis, qualitative amine tests were performed to determine the completion of coupling reactions.[29] The reagents of the qualitative amine test were three kinds of solutions: 5% ninhydrin in ethanol (w/v), 80% phenol in ethanol (w/v) and 2 mL

0.001 M potassium cyanide in 98 mL pyridine. After the coupling reaction was done, a few resin beads were transferred to a small test tube and 3 drops of each of the solutions above were added into the beads. The solution was mixed well and heated to 120°C for 4 to 6 minutes. A positive result was shown by the colorless solution, which indicated the absence of resin-bound free amine. If the solution became blue, the coupling reaction was not complete yet.

2.5.2 Synthesis of DOTA-Ahx-Orexin B Analogue (3 & 4)

The synthetic procedure of Ahx-orexin A (15-33) and Ahx-orexin B (6-28) was the same as the peptide synthetic procedure described above. After the coupling of Fmoc-Ahx to the peptide chains, DOTA-tris (*t*Bu)-ester (0.2 mmol) dissolved in 2 mL DMF with DIPEA (0.4 mmol) and HBTU (0.2 mmol) was added into the resin, shaking for 24 hours at room temperature. The procedures of full cleavage, purification and analysis of DOTA-Ahx-orexin were the same as described above.

2.5.3 Synthesis of Ga-DOTA-Ahx-Orexin A/B Analogues (12 & 13)

Gallium nitrate (10 equiv.) was added into DOTA-Ahx-orexin A (15-33) (**9**) (2 mg) or DOTA-Ahx-orexin B (6-28) (**10**) (2 mg) in 1 mL HOAc / NaOAc buffer (pH~5). The solution was heated at 70°C for 10 minutes. After the reaction was complete, the resulting compounds were purified by RP-C18 SPE sep-pak© cartridge. The sep-pak© was rinsed with 5 mL anhydrous EtOH and then 10 mL H_2O. After passing the reaction mixture through the sep-pak©, 10 mL H_2O was used as the eluent to wash out the unreacted $Ga(NO_3)_3$ and HOAc / NaOAc buffer. Then 5 mL EtOH was used to wash out the gallium

labelled orexin A (15-33) or orexin B (6-28). The sep-pak© eluate was evaporated and lyophilized to yield white powders **12** or **13**.

2.5.4 ^{68}Ga Radiolabelling of DOTA-Ahx-Orexin A/B Analogues (8 & 11)

DOTA-Ahx-orexin A (15-33) (**9**) (1 mg) or DOTA-Ahx-orexin B (6-28) (**10**) (1 mg) was dissolved in 1 mL NaOAc/ HOAc buffer (pH~5). The solution of 1.61 mCi ^{68}GaCl$_3$ in diluted HCl was added to 0.1 mL of the peptide solution. The reaction mixture was heated at 70°C for compound **9** or 90°C for compound **10** for 20 minutes. Before purification, the sep-pak© was rinsed with 5 mL anhydrous EtOH and then10 mL H$_2$O. After passing the reaction mixture through the sep-pak©, 10 mL H$_2$O was used as the eluent to wash out the unreacted ^{68}GaCl$_3$ and HOAc / NaOAc buffer. Then 5 mL EtOH was used to wash out the ^{68}Ga labelled DOTA-Ahx-orexin A (15-33) or DOTA-Ahx-orexin B (6-28). The sep-pak eluate was evaporated on a rotary evaporator to give **8** or **11**. They were analyzed by RP-HPLC equipped with a gamma detector.

References

(1)   Delecea, L.; Kilduff, T. S.; Peyron, C.; Gao, S. B., Foye, P. E.; Danielson, P. E. et al. *National Academy of Sciences* **1998**, *95*, 322.

(2)   Sakurai, T.; Amemiya, A.; Ishii, M.; Matsuzaki, I.; Chemelli, R. M.; Tanaka, H. et al. *Cell* **1998**, *92*, 537.

(3)   Tsujino, N.; Sakurai, T. *Pharmacological Reviews* **2009**, *61*, 162.

(4)   Shibahara, M.; Sakurai, T.; Nambu, T.; Takenouchi, T.; Iwaasa, H.;

Egashira S. I. et al. *Peptides* **1999**, *20*, 1169.

(5)   Alvarez, C. E.; Sutcliff, J. G. *Neuroscience Letters* **2002**, *324*, 169.

(6)   Miskolzie, M.; Kotovych, G. *Biomolecular Structure & Dynamics* **2003**, *21*, 201.

(7)   Kim, H. Y.; Hong, E.; Kim, J.; Lee, W. *Journal of Biochemistry and Molecular Biology* **2004**, *37*, 565.

(8)   Takai, T.; Takaya, T.; Nakano, M.; Akutsu, H.; Nakagawa, A.; Aimoto, S. et al. *Journal of Peptide Science* **2006**, *12*, 443.

(9)   Lee, J. H.; Bang, E.; Chae, K. J.; Kim, J. Y.; Lee, D. W.; Lee, W. *European Journal of Biochemistry* **1999**, *266*, 831.

(10)   Darker, J. G.; Porter, R. A.; Eggleston, D. S.; Smart, D.; Brough, S. J.; Sabido-David, C. et al. *Bioorganic & Medicinal Chemistry Letters* **2001**, *11*, 737.

(11)   Lang, M.; So, R. M.; Dürrenberger, F.; Dautzenberg, F. M.; Beck-Sickinger, A. G. *Journal of Medicinal Chemistry* **2004**, *47*, 1153.

(12)   Lee, S.; Xie, J.; Chen, X. *Biochemistry* **2010**, *49*, 1364.

(13)   Voison, T.; Rouet-Benzineb, P.; Reuter, N.; Laburthe, M. *Cellular and Molecular Life Sciences* **2003**, *60*, 72.

(14)   Jöhren, O.; Neidert, S. J.; Kummer, M.; Dendorfer, M.; Dominiak, P. *Endocrinology* **2001**, *142*, 3324.

(15)   Liu, M.; Kirchgessner, A. L. *Neuron* **1999**, *24*, 941.

(16)   López, M.; Señaris, R.; Gallego, R.; García-Caballero, T.; Lago, F.; Seoane, L. et al. *Endocrinology* **1999**, *140*, 5991.

(17)   Blanco, M.; López, M.; García-Caballero, T.; Gallego, R.; Vázquez-

Boquete, Á.; Morel, G. *Journal of Clinical Endocrinology & Metabolism* **2001**, *86*, 3444.

(18)   Tafuri, S.; Pavone, L. M.; Muto, R. L.; Basile, M.; Langella, E.; Riorillo, E. et al. *Regulatory Peptides* **2009**, *15*, 1.

(19)   Ouedraogo, R.; Näslund, E.; Kirchgessner, A. L. *Diabetes* **2003**, *52*, 111.

(20)   Rouet-Benzineb, P.; Rouyer-Fessard, C.; Jarry, A.; Avondo, V.; Cécile, P.; Yanagisawa, M. et al. *The Journal of Biological Chemistry* **2004**, *279*, 45875.

(21)   Voisin, T.; Firar, A. E.; Fasseu, M.; Rouyer-Fessard, C.; Descatoire, V.; Walker, F. et al. *American Association for Cancer Research* **2011**, *71*, 3341.

(22)   Weissleder, R.; Ntziachristos, V. *Nature Medicine* **2003**, *9*, 123.

(23)   Liu, Y.; Liu, G.; Hnatowich, D. J. *Materials* **2010**, *3*, 3204.

(24)   Bartholoma, M. D.; Louie, A. S.; Valliant, J. F.; Zubieta, J. *Chemical Reviews* **2010**, *110*, 2903.

(25)   Bauwens, M.; Chekol, R.; Vanbilloen, H.; Bormans, G.; Verbruggen, A. *Nuclear Medicine Communications* **2010**, *31*, 753.

(26)   Velikyan, I. PhD. Dissertation, Uppsala University, 1998.

(27)   Langstrom, B.; Bergson, G. *Radiochemical and Radioanalytical Letters* **1980**, *43*, 47.

(28)   Liu, S. *Chemical Society Reviews* **2004**, *33*, 445.

(29)   Chan, W. C.; White, P. D. In *Fmoc Solid Phase Peptide Synthesis*; Chan, W. C.; White, P. D., Eds.; Oxford University Press: New York, 2003.

Chapter 3   Optimization of AEEA Linker Synthesis

3.1   Introduction

In the design of molecular imaging probes, a linker can be incorporated between the targeting entity and the imaging moiety to minimize the effects of the imaging moiety on the biological binding activities of the targeting entity toward its target.[1] Figure 3.1 shows some examples of linkers which have been used in the design of molecular imaging probes.[2-6] The linker can be a synthesized amphiphilic molecule such as PEG (**14**), a natural amino acid such as lysine (**15**) or an amino acid sequence such as Gly-Gly-Gly (**16**). The PEG linker (**14**) represents a large number of possible molecules, formed by linking repeating units of ethylene oxide.[7] These PEG moieties can be produced in different configurations (linear or branched structures) and different molecular weights to optimize the properties of the imaging probes, such as increasing the binding affinity and enhancing the water solubility.[7]
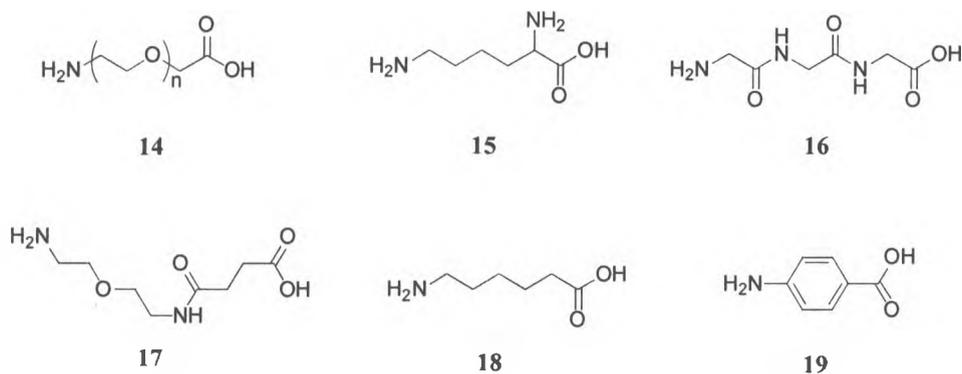
Figure 3.1   Structures of linkers: poly ethylene glycol (PEG) (**14**), lysine (**15**), Gly-Gly-Gly sequence (**16**), 5-amino-3-oxapentyl-succinamic acid (**17**), aminohexanoic acid (ahx) (**18**) and *p*-aminobenzoic acid (**19**).

In 2009, Liu Z. et al. synthesized a ^{68}Ga labelled cyclic RGD dimer ((RGD)$_2$), with 1,4,7-triazacyclononanetriacetic acid (NOTA) as the chelator, targeting glioma cells.[8] They found that the use of the PEG$_4$ linker and Gly$_3$ (Gly-Gly-Gly) linker could increase the binding affinity of NOTA conjugated RGD dimer (Figure 3.2). The IC$_{50}$ value of NOTA-(RDG)$_2$ (**20**) without a linker was 100 nM.[8] However, after the incorporation of the Gly$_3$ linker, the IC$_{50}$ value of NOTA-(Gly$_3$-RDG)$_2$ (**21**) was decreased to 66 nM.[8] After the displacement of Gly$_3$ by PEG$_4$, the IC$_{50}$ value of NOTA-(PEG$_4$-RDG)$_2$ (**22**) was lowered to 40 nM.

Figure 3.2 The structures of compounds **20**, **21** and **22**. The RGD (Arg-Gly-Asp) sequence strongly binds to the integrin $\alpha_v\beta_3$ receptor, which is overexpressed in several tumor types including lung carcinoma and breast cancer.[1]

The use of linkers may also reduce the spatial hindrance to improve the labeling yield of imaging probes.[9] Wu Z. et al. demonstrated that the introduction of the PEG_3 linker increased the fluorine-18 radiolabeling yield of tetrameric RGD peptide due to reduced steric effect (Figure 3.3). The coupling yield between PEG_3-$(RGD)_4$ and ^{18}F-SFB (N-succinimidyl 4-[^{18}F]fluorobenzoate) was above 20%, while the yield for the same coupling reaction between $(RGD)_4$ and ^{18}F-SFB without PEG_3 linker was less than 2%.[9]
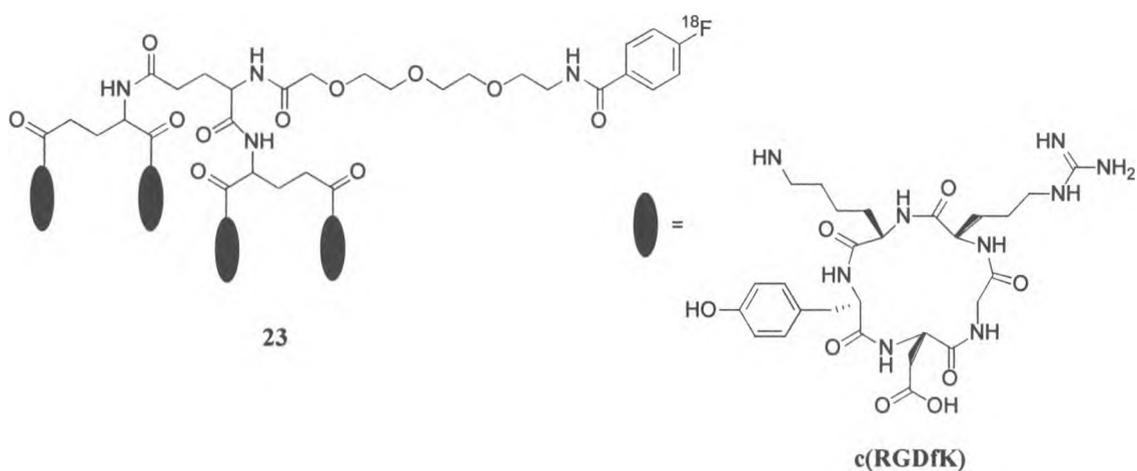
Figure 3.3 The structure of ^{18}F labelled PEG-$(RGD)_4$ (**23**).[9]

In addition, the incorporation of a linker may alter the pharmacokinetic property of an imaging probe. Garrison J. C. et al. studied the pharmacokinetic effects of various linkers using indium-111 radiolabelled bombesin (7-14).[4] Bombesin (BBN) is an amphibian homologue of mammalian gastrin-releasing peptide (GRP).[10] It has high binding affinity to GRP receptor (GRPr), which is overexpressed in several tumors including prostate,

breast and gastrointestinal tumors.[10,11] As a result, various BBN analogues have been developed as potential imaging probes targeting cancer cells, such as prostate cancer. Garrison J. C. et al. synthesized six radioconjugates ^{111}In-DOTA-**X**-BBN (7-14)-NH$_2$ with different linkers (**X** = 8-aminooctanoic acid (8-AOC), 5-amino-3-oxapentyl-succinamic acid (5-ADS), 8-amino-3,6-dioxaoctyl-succinamic acid (8-AOS), *p*-aminobenzoic acid (AMBA), Gly-AMBA, and Gly-*p*-aminomethylbenzoic acid (Gly-AM2BA)) (Figure 3.4).[4] Their study indicated that the imaging probes containing aromatic linkers exhibited higher *in vivo* tumor uptake and retention than the ether and hydrocarbon linkers.[4]

[111]**In-DOTA-X-BBN (7-14)-NH$_2$**
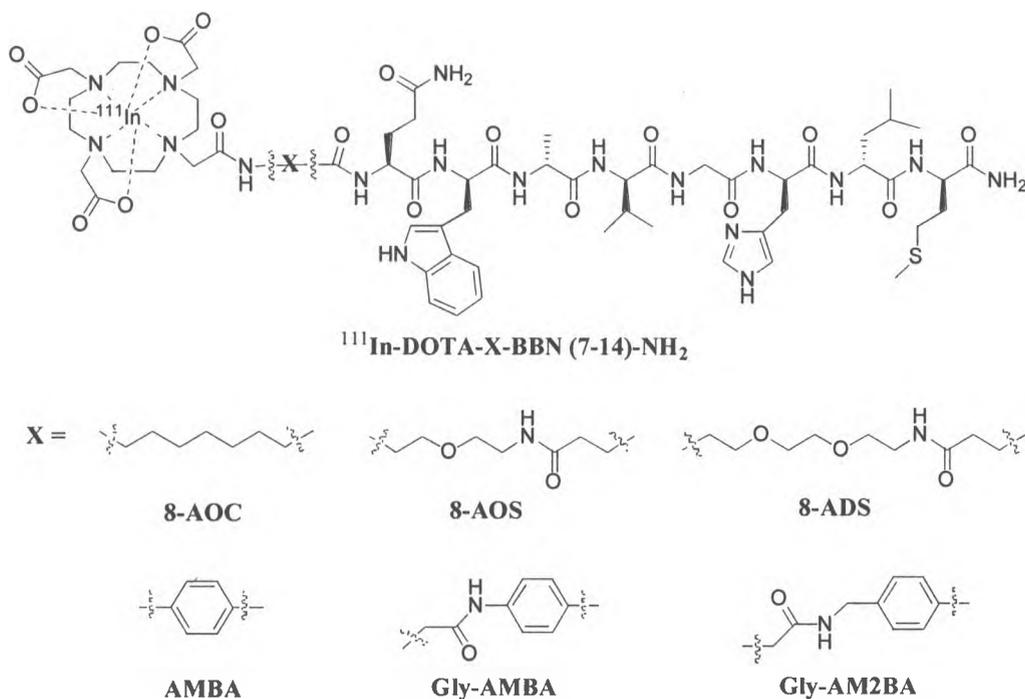
Figure 3.4 Structures of ^{111}In labelled BBN analogues.[4]

3.2 Objective

Orexin A and orexin B had poor solubility in water, especially when they were labelled with FITC. Compared to the linker aminohexanoic acid, [2-(2-amino-ethoxy)-ethoxy]-acetic acid (AEEA) linker is more hydrophilic, so the introduction of an AEEA linker between the orexin peptide and FITC molecule might improve the water solubility of FITC labelled orexin based imaging agents. AEEA is a PEG moiety, which is an inert amphiphilic molecule comprising two units of ethylene oxide. Although the synthesis of Fmoc-AEEA (24) has been published in a patent, the yield was low in our hands.[12] This project aimed to try different methods to improve the yield of Fmoc-AEEA synthesis.
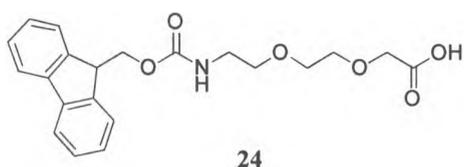
Figure 3.5 The structure of Fmoc-AEEA (24).

3.3 Results and Discussion

A synthetic procedure of Fmoc-AEEA (24) was provided in the patent literature as described in Scheme 3.1 and started with commercially available 2-[2-(2-chloro-ethoxy)-ethoxy]-ethanol (25).[12] After the reaction with sodium azide, triphenylphosphine, water and Fmoc-Cl, [2-[2-(Fmoc-amino) ethoxy] ethoxy]-ethanol (29) was formed (Scheme 3.1). Then with 2,2,6,6-tetramethylpiperidine-1-oxyl (TEMPO) as the catalyst and sodium hypochlorite as the oxidant, compound 29 was oxidized into 24 (Scheme 3.2).

However, in our hands the synthesis of Fmoc-AEEA using the method provided by this patent gave a very low yield of 26% as compared to the published value of 80%. It was found that the low yield was due to the inefficient oxidation from compound **29** to **24**, which is shown in Scheme 3.2.
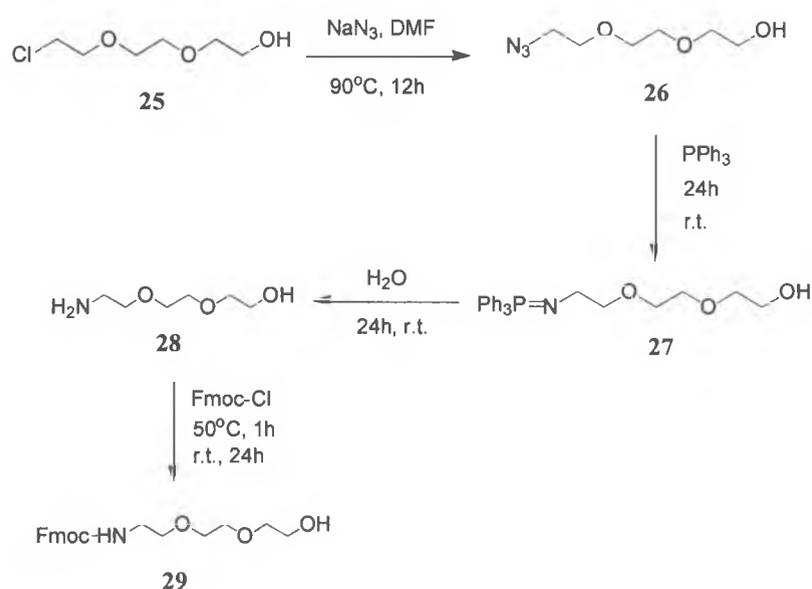
Scheme 3.1 Synthetic procedure of [2-[2-(Fmoc-amino) ethoxy] ethoxy] ethanol (**29**).[12]
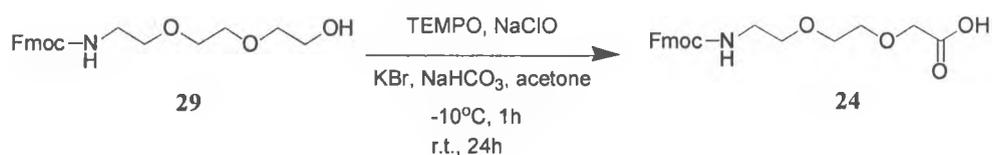
Scheme 3.2 Synthetic procedure of Fmoc-AEEA (**24**).[12]

52

In order to improve the yield of Fmoc-AEEA synthesis, two additional oxidation methods were attempted. It has been reported that the addition of sodium chlorite could improve the yield of TEMPO/NaClO oxidation.[13] When sodium chlorite was used in the Fmoc-AEEA synthesis, the overall yield was improved to 45% (Scheme 3.3). Compared to the oxidation reaction without sodium chlorite, the yield was increased significantly.
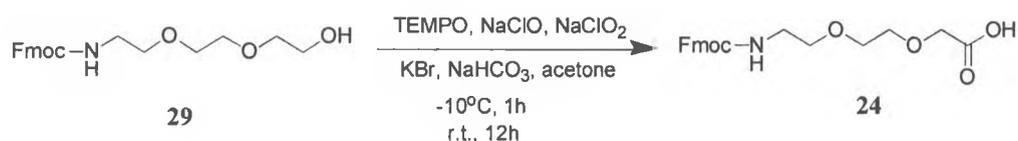
Scheme 3.3 The procedure of Fmoc-AEEA synthesis by TEMPO, NaClO and NaClO$_2$.

Another oxidant, Jones reagent, a solution of chromium trioxide in dilute sulphuric acid, was attempted to oxidize **29** to **10** as well (Scheme 3.4). Jones reagent resulted in a great increase in the yield of Fmoc-AEEA synthesis, which was 63%, much higher than the yields of the two methods described previously.
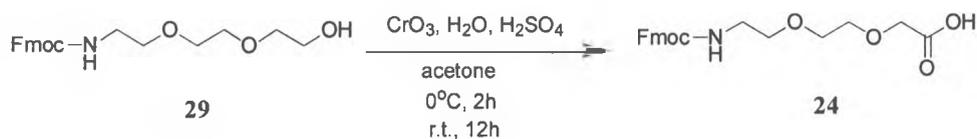
Scheme 3.4 The synthetic procedure of Fmoc-AEEA using Jones oxidation.

3.4 Conclusion

Among all the three oxidation methods described above, there was an advantage to use the TEMPO/NaClO/NaClO$_2$ method. Compared to the TEMPO/NaClO method (26%), the TEMPO/NaClO/NaClO$_2$ method gave a much higher yield (45%). Although its yield was lower than that given by the method of Jones oxidation (64%), it was easier to work up and safer. Jones reagent contained chromium which might cause pollution to the environment, so the waste from this reaction must be disposed of carefully. The synthesized Fmoc-AEEA was used in the design of orexin based imaging agents. Fluorescein-AEEA-orexin A (15-33) (2) and fluorescein-AEEA-orexin B (6-28) (4) were made successfully and the solubility of these two imaging agents was slightly improved.

3.5 Experimental

Sodium hypochlorite was purchased from Queen Bleach Co. Limited in Mississauga. Sodium azide was obtained from EMD Chemicals in Gibbstown. Fmoc-Cl was provided by Advanced ChemTech in Louisville. All the other reagents and solvents were purchased from Sigma-Aldrich and used without further purification. Analytical TLC was performed on EMD silica gel 60 F$_{254}$ plates and column chromatography was carried out by Merck silica gel 60 (230-400 mesh). ^{1}H and ^{13}C NMR data were obtained by Varian Mercury 400 at 25°C and the chemical shifts were referenced to solvent signals (CDCl$_3$: ^{1}H 7.27 ppm, ^{13}C 77.00 ppm) relative to TMS. Mass spectra were obtained from a Finnigan MAT 8200 mass spectrometer.

Synthesis of Fmoc-AEEA (24)

Step 1: Synthesis of [2-[2-(Fmoc-amino) ethoxy] ethoxy] ethanol (**29**)

29
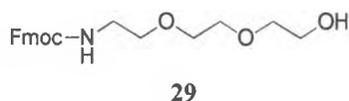
2-[2-(2-chloro-ethoxy)-ethoxy]-ethanol (**25**) (3.25 g, 19.4 mmol), sodium azide (1.25 g, 19.4 mmol), and 25 mL dry *N,N*-dimethylformamide were added into a 100-mL round-bottom flask. The mixture was stirred overnight at 90°C under nitrogen, cooled to room temperature and diluted with 100 mL of dry tetrahydrofuran. Sodium chloride precipitated out and was removed by vacuum filtration quickly. Triphenylphosphine (5.60 g, 20.9 mmol) was added into the filtrate in two batches over 15 minutes under nitrogen. After stirring for 24 hours, 1.5 equivalent of water (0.6 mL) was added and the mixture was stirred for another 24 hours. The solvents (THF and DMF) were evaporated by the rotary evaporator and then an oily liquid was recovered. To this was added 40 mL water and the precipitated solid was removed by filtration. After washing the solid with 3 x 5 mL water, sodium carbonate (5.50 g, 19.4 mmol) was added to the filtrate and the solution was kept cool in a water/ice bath. To the cold solution, Fmoc-Cl (5.00 g, 19.4 mmol) dissolved in 25 mL THF was added dropwise over 30 minutes. The reaction was stirred at 50°C for 1 hour and then at room temperature overnight. After THF was evaporated, [2-[2-(Fmoc-amino) ethoxy] ethoxy] ethanol (**29**) was extracted out from the aqueous layer with ethyl acetate (6 x 50 mL). The extract was dried with MgSO$_4$ and then MgSO$_4$ was removed by filtration. The filtrate was evaporated to get a light yellow oil **29**. A small amount of this oil was purified by column chromatography (20% ethyl acetate in

hexane). ^{1}H NMR (400 MHz, CDCl$_3$, 25°C): δ/ppm 7.78-7.75 (m, 2H), 7.62-7.60 (m, 2H), 7.42-7.38 (m, 2H), 7.34-7.29 (m, 2H), 5.53 (bs, 1H), 4.44-4.41 (m, 2H), 4.23 (t, J = 4 Hz, 1H), 3.74-3.50 (m, 10H), 3.41-3.39 (m, 2H). MS-EI: 371.1717 m/z (calc: 371.1733 m/z).

Step 2': Synthesis of Fmoc-AEEA (**24**) by TEMPO/NaClO

24
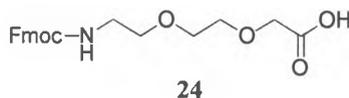
Acetone (95 mL) was added to the crude oil **29** (7.20 g, 19.4 mmol) obtained from step 1 and the solution was cooled to -10°C in an iso-propanol/dry ice bath. 5% sodium bicarbonate solution (95 mL) was added to the cold solution, followed by KBr (0.225 g, 1.9 mmol) and TEMPO (3.40 g, 22 mmol). To this mixture NaOCl solution (30.0 mL, 25.6 mmol, 5.25%) was added dropwise over 10 minutes. After 1 hour, additional NaOCl (14.3 mL, 12.2 mmol, 5.25%) was added over 5 minutes. The reaction was stirred below 0°C for another 1 hour, then at room temperature overnight. Acetone was evaporated by the rotary evaporator, and the light-yellow solution was extracted with ethyl acetate (6 x 50 mL) until the aqueous layer became colorless. The aqueous solution was acidified with 1M HCl in a water/ice bath until a precipitate formed (pH~2). The mixture was stored in the fridge overnight. The resulting precipitate was filtered and dried over vacuum for 2 days to get the final product as a white powder **24** (1.95 g, overall yield 26.1%). ^{1}H NMR (400 MHz, CDCl$_3$, 25°C): δ/ppm 7.77(d, J = 8 Hz, 2H), 7.61 (d, J = 8 Hz, 2H), 7.42-7.39 (m, 2H), 7.34-7.30 (m, 2H), 5.32 (bs, 1H), 4.41 (d, J = 4 Hz, 2H), 4.23 (t, J = 8 Hz, 1H), 4.17 (s, 2H), 3.76-3.42 (m, 8H). ^{13}C NMR (400 MHz, CDCl$_3$,

25°C): δ/ppm 172.53, 156.64, 143.91, 141.29, 127.67, 127.05, 125.08, 119.95, 71.31, 70.31, 69.99, 68.61, 66.78, 47.20, 40.77. MS-EI: 385.1537 m/z (calc: 385.1525 m/z).

Step 2'': Synthesis of Fmoc-AEEA (**24**) by TEMPO/NaClO/NaClO$_2$
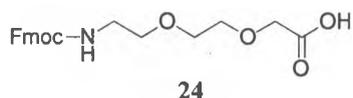
24

Acetone (30 mL) was added to the crude oil **29** (2.23 g, 6.0 mmol) obtained from step 1 and the solution was cooled to -10°C in an iso-propanol/dry ice bath. 5% sodium bicarbonate solution (30 mL) was added to the cold solution, followed by KBr (0.07 g, 0.6 mmol), and TEMPO (1.05 g, 6.7 mmol). To this mixture, 0.7 g NaClO$_2$ (8.0 mmol) dissolved in 10 mL water was added dropwise over 10 minutes, and then NaClO (9.4 mL, 8.0 mmol 5.25%) was added dropwise over 10 minutes. After 1 hour, additional NaClO$_2$ solution (5 mL, 6.54%) was added over 5 minutes, followed by additional NaClO (4.5 mL, 8.0 mmol, 5.25%). The reaction was stirred below 0°C for another 1 hour, then at room temperature overnight. Acetone was evaporated and the light-yellow solution was extracted with ethyl acetate (6 x 15 mL) until the aqueous layer became colorless. The aqueous solution was acidified with 1M HCl in a water/ice bath until there was a precipitate formed (pH~2). The mixture was stored in the fridge overnight. The resulting precipitate was filtered and dried over vacuum for 2 days to get the product as a white powder **24** (1.15 g, overall yield 49.8%). The white powder was recrystallized with ethanol/H$_2$O (3:1) to get the final pure product (1.04 g, overall yield 45.2%).

Step 2''': Synthesis of Fmoc-AEEA (**24**) by Jones oxidation
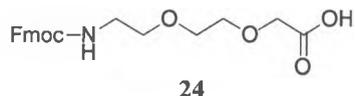
24

Acetone (30 mL) was added to the crude oil **29** (2.23 g, 6.0 mmol) obtained from step 1 and the solution was cooled to $0^{\circ}C$ in a water/ice bath. Fresh Jones reagent (prepared by dissolving 1.19 g CrO_3 in 16 mL water and then adding 2.2 mL H_2SO_4) was added to the mixture, which was stirred at $0^{\circ}C$ for 2 hours and then at room temperature overnight. Iso-propanol was used to quench the reaction. Acetone and iso-propanol were evaporated to obtain a green-yellow oil. The crude product was purified by column chromatography (2% methanol in chloroform, 1% acetic acid). After purification, 1.45 g **24** was obtained and the overall yield was 62.8%.

References

(1)   Lee, S.; Xie, J.; Chen, X. Y. *Chemical Reviews* **2010**, *110*, 3087.

(2)   Brillouet, S.; Dorbes, S.; Courbon, F.; Picard, C.; Delord, J. P.; Benoist, E. et al. *Bioorganic & Medicinal Chemistry* **2010**, *18*, 5400.

(3)   Azad, B. B.; Rota, V. A.; Breadner, D.; Dhanvantari, S.; Luyt, L. G. *Bioorganic & Medicinal Chemistry* **2010**, *18*, 1265.

(4)   Garrison, J. C.; Rold, T. L.; Sieckman, G. L.; Naz, F.; Sublett, S. V.; Figueroa, S. D. et al. *Bioconjugate Chemistry* **2008**, *19*, 1803.

(5)   Parry, J. J.; Kelly, T. S.; Andrews, R.; Rogers, R. E. *Bioconjugate Chemistry* **2007**, *18*, 1110.

(6)   Dijkgraaf, I.; Liu, S.; Kruijtzer, J. A. W.; Soede, A. C.; Oyen W. J. G.; Liskamp R. M. J. et al. *Nuclear Medicine and Biology* **2007**, *34*, 29.

(7)   Harris, J. M.; Martin, N. E.; Modi, M. *Clinical Pharmacokinetics* **2001**, *40*, 539.

(8)   Liu, Z.; Niu, G.; Shi, J.; Liu, S.; Wang, F.; Liu, S. et al. *European Journal of Nuclear Medicine & Molecular Imaging* **2009**, *36*, 947.

(9)   Scott, W.; Anjali, S.; Mond, J. *Antimicrobial Agents and Chemotherapy* **2003**, *47*, 554.

(10)   Smith, C. J.; Volkert, W. A.; Hoffman, T. J. *Journal of Nuclear Medicine* **2005**, *32*, 733.

(11)   Reubi, J. C. *Endocrine Reviews* **2003**, *24*, 389.

(12)   Aldrich, J. V.; Kumar, V. U.S. Patent, US20030134989A1, July 17, 2003.

(13)   Zhao, M. M.; Li, J.; Mano, E.; Song, Z. J.; Tschaen, D. M. *Organic Syntheses* **2005**, *81*, 195.

Chapter 4 Design of Orexin Receptor Antagonists as Imaging Agents

4.1 Introduction

4.1.1 Biological Functions of Orexin Systems

Orexin peptides and their receptors are expressed in the lateral hypothalamus and adjacent areas, a region regulating feeding behavior and energy homeostasis.[1-4] It is the reason that orexin was named after "orexis", which means appetite in Greek. In 1998, Sakurai et al. demonstrated that orexin A and orexin B can stimulate food intake in a dose-dependent way.[1] They also found that the production and release of orexin peptides were affected by the nutritional state of animals. Within 48h fasting, hypothalamic prepro-orexin mRNA was in a 2.4-fold up-regulation compared with the fed control animals. Further evidence indicated that the increase of food consumption resulted from the delay of the onset of a normal satiety sequence via the activation of orexin receptors by orexin receptor agonists (orexin A and orexin B), while an orexin receptor antagonist inhibited food consumption and accelerated the onset of a normal satiety sequence.[5]

Further research found that orexin deficiency contributes to narcolepsy in humans and animals, which indicates that orexin plays a significant role in regulation of the sleep-wake cycle.[6-11] The study discovered that a long, consolidated awake period was maintained due to the activation of wake-active neurons in the hypothalamus and brain

stem by orexin.[6] It was also reported that the orexin A level in the cerebrospinal fluid was decreased in approximately 90% of patients with narcolepsy, especially those with narcolepsy-cataplexy.[12] As a result, the 2nd edition of the international classification of sleep disorders introduced a low cerebrospinal fluid level of orexin A as one of the diagnostic criteria for narcolepsy-cataplexy.[13]

4.1.2 Development of Orexin Receptor Antagonist

Since orexin participates in the regulation of food-intake and sleep-wakefulness, many orexin receptor antagonists have been developed as potential drugs for the treatment of insomnia and obesity. Based on their binding affinities to orexin receptors, the orexin receptor antagonists can be divided into two groups: selective orexin receptor antagonist (SORA) and dual orexin receptor antagonist (DORA). Many of these orexin receptor antagonists have very low IC_{50} values, even below 1 nM, much lower than those of the orexin receptor agonists orexin A and orexin B (Table 4.1 & 4.2).

Table 4.1 The IC_{50} values of orexin receptor agonists (orexin A and orexin B).[14]

Agonist	IC_{50} at OX_1R (nM)	IC_{50} at OX_2R (nM)
Orexin A	20	250
Orexin B	20	20

Table 4.2 The IC_{50} values of some orexin receptor antagonists.[14-16]

Antagonist	Structure	IC_{50} at OX_1R (nM)	IC_{50} at OX_2R (nM)
30		0.71	0.08
31		26	6
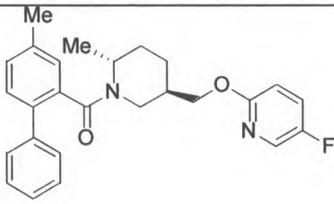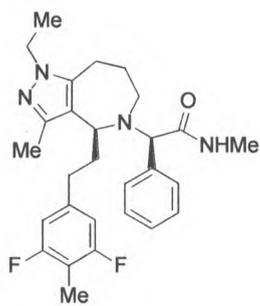
The first published orexin receptor antagonist is SB-334867-A (**32**), which binds to OX_1R selectively (Figure 4.1).[17] It was demonstrated that **32** could reduce the food intake and body weight and has a potential clinical application in the treatment of obesity.[18] To date, there are three dual orexin receptor antagonists studied in clinical trials: Almorexant (**33**), SB-649869 (**34**) and MK-4305 (**35**) (Figure 4.1).[19] Compound **33** was developed based on the tetrahydroisoquinoline motif by Actelion Pharmaceuticals.[20] It has been proven that **33** can reduce wakefulness in rats, dogs, and humans without cataplexy.[21] It also improved the sleep initiation and sleep maintenance of insomnia patients without significant next-day effects on motor function in a Phase II study.[20] However, the Phase III study was abandoned because of undesirable side effects. SB-649869 (**34**), a derivative of *N*-acyl piperidine, was developed by SmithKline Beecham.[15] Although it

showed positive results in sleep efficacy, its development was delayed due to preclinical toxicology findings.[19] In 2008, Merck claimed substituted diazepane derivatives as orexin receptor antagonists, one of which was compound **35**. The preliminary Phase I result of **35** showed decreased latency to persistent sleep and wake after sleep onset in healthy volunteers.[19,22]



32

33

34

35
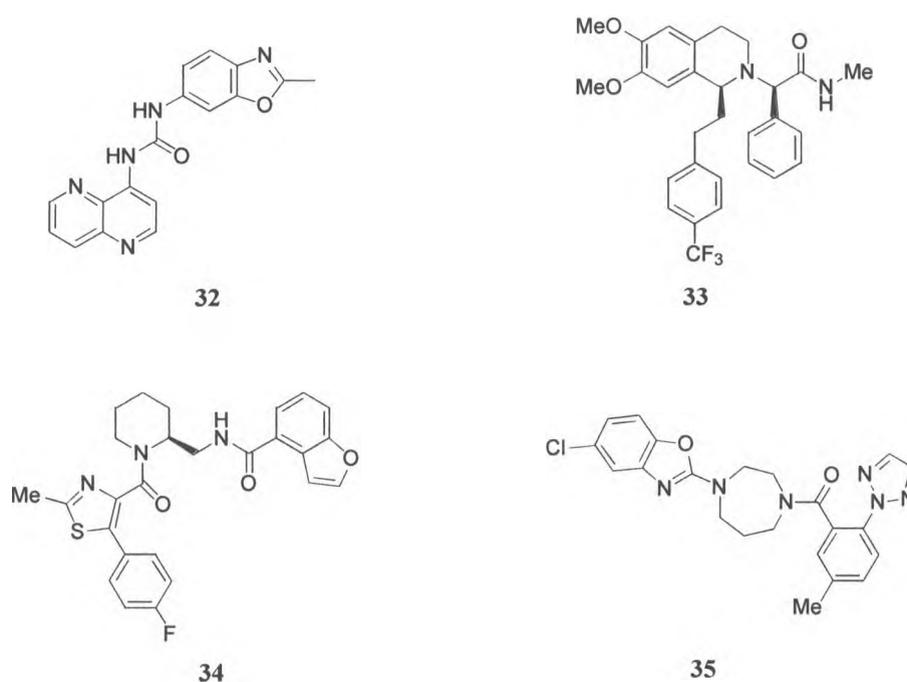
Figure 4.1 The structures of SORA SB-334867 (**32**) and DORAs Almorexant (**33**), SB-649869 (**34**) and MK-4305 (**35**).[19]

4.1.3 Substituted Diazepane Orexin Receptor Antagonists

In 2009, Merck & Co. Pharmaceuticals published a series of orexin receptor antagonists based on the substituted diazepane motif. Many of those antagonists have an IC_{50} value below 100 nM. Compound **36** is one of those antagonists with a rather low IC_{50} value (OX_1R IC_{50} = 29 nM, OX_2R IC_{50} = 27 nM) (Figure 4.2).[23]
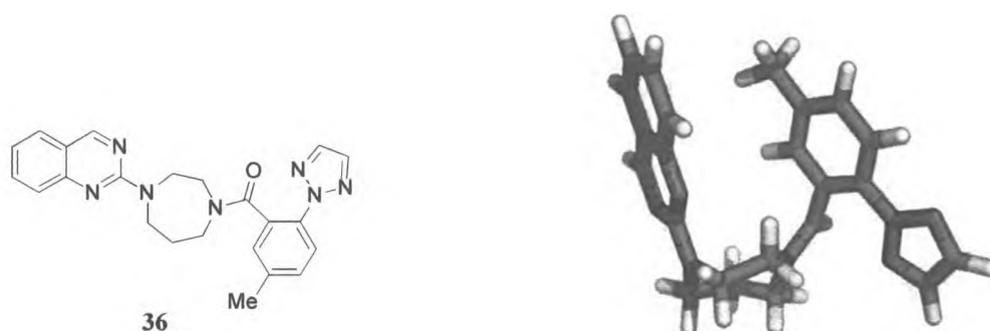

Figure 4.2 Structure and X-ray structure of **36**.[23]

As shown in Figure 4.2, compound **36** adopts a twist-boat ring conformation with an intramolecular π-stacking interaction. It was concluded that the twist-boat ring and low-energy conformation of *N,N*-disubstituted-1,4-diazepane orexin receptor antagonists resulted in a reduced conformational entropy, in order to resemble the conformation of the required binding orientation.[24] To investigate the role of π-stacking interaction in the biological binding activity, compound **37** (cyclohexyl amide instead of benzoic amide) was synthesized (Table 4.3).[24] Without the intramolecular π-stacking interaction in **37**, the binding affinity was decreased. The compounds **38** (2-naphthyl analog) and **39** (tertiary amine instead of amide carbonyl) were synthesized to study the binding affinity as well.[24] Through the comparison of binding affinities, it was discovered that the

quinazoline ring was slightly better than the naphthalene ring and the amide carbonyl was much better than a tertiary amine.

Table 4.3   The binding affinities of *N,N*-disubstituted-1,4-diazepane orexin receptor antagonists.[24]

Compound	Structure	OX$_1$R Ki (nM)	OX$_2$R Ki (nM)
36		1.2	0.6
37		9800	550
38		2	2
39		930	240
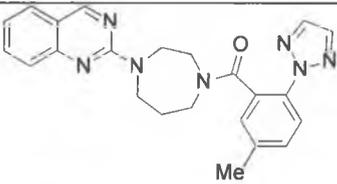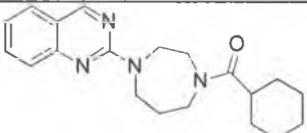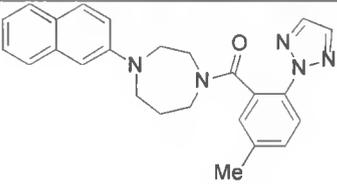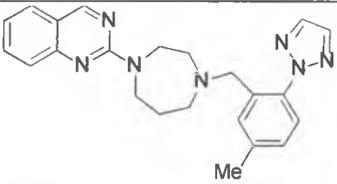
4.1.4   Fluorine-18 Labelled Imaging Agents

In the past 20 years, many fluorine-18 labelled radiopharmaceuticals have been introduced for human studies, such as 2-deoxy-2-[^{18}F]fluoro-D-glucose ([^{18}F]FDG) (**40**), which can be utilized as an imaging probe for the diagnosis of cancer.[25] Fluorine has a small atomic radius and forms a strong carbon-fluorine bond, which is the strongest covalent bond in organic chemistry.[26] Due to the small steric size of fluorine, the molecular size of imaging agents labelled by fluorine-18 does not change significantly, which might minimize the effects of imaging labels on the biological binding affinities. Substitution with fluorine can also change the physiochemical and biological properties of the organic compound significantly and usefully.[25] Because the carbon-fluorine bond is more hydrophobic than the carbon-hydrogen bond, the fluorine addition to biologically active organic compounds may increase the lipophilicity resulting in an increased cell membrane penetration.[27] Also, the stability of the carbon-fluorine bond may slow down the metabolism of radiopharmaceuticals, giving a longer time for imaging.

One of the popular fluorine radiotracers is [^{18}F]FDG (**40**), which was developed to study glucose metabolism in the human brain in 1976.[25] Later research demonstrated that there was a high uptake of **40** in the rapidly growing tumors resulting from increased tumor glycolysis.[28,29] To date, many hospitals have used **40** for clinical diagnosis via molecular imaging in heart disease and in oncology.[25] Figure 4.3 shows the image of a [^{18}F]FDG PET scan of a 78-year-old woman with colorectal cancer.[30] The detection of tumors by a [^{18}F]FDG PET scan in many instances is more accurate than the CT scan. Among the 38 patients with colorectal cancer studied by Kantorová Iva in 2003, 95% of primary tumors were detected by [^{18}F]FDG PET, while CT only detected 49% of primary tumors.[30]
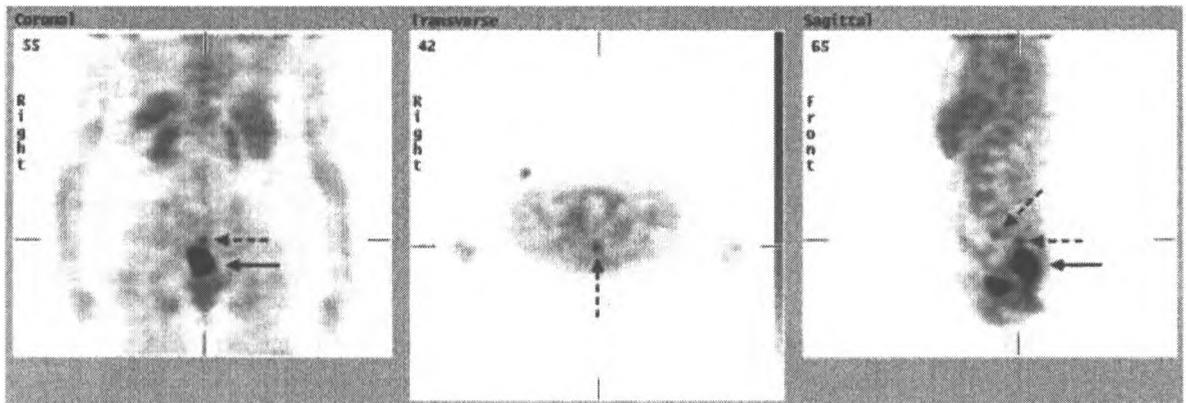
Figure 4.3 [^{18}F]FDG PET scan of a 78-year-old woman with primary rectal carcinoma (solid arrows) and histologically proven metastasis in lymph nodes (dashed arrows).[30]

4.2 Objective

It has been established that PET imaging has a significant role in evaluating and staging recurrent colorectal cancer in patients with **40** as the imaging probe.[31] Although [^{18}F]FDG imaging is quite sensitive in the detection of tumors, the high FDG uptake is not only specific for tumors.[32] Inflammatory processes may also cause an increased uptake of FDG, resulting in false-positive results, which have been reported in tuberculosis, presacral abscesses and fungal infections.[31] The non-specificity of [^{18}F]FDG imaging in the detection of colorectal tumors requires the development of new imaging probes.

As described in Chapter 2, OX_1R is expressed in colon cancer cells but not in normal colonic epithelial cells, which led to the idea of designing [^{18}F]fluorinated orexin receptor antagonists as potential imaging probes targeting colon cancer cells.[33] Many orexin receptor antagonists have been developed in the past ten years and many of them have high binding affinities to OX_1R. After evaluating all of them, the substituted diazepane orexin receptor antagonists attracted our attention. Those antagonists have low IC_{50} values and great potential to be labelled by fluorine-18 based on the techniques and the accessibility of equipment in our laboratory.

As a result, we designed [^{18}F](4-fluoro-phenyl)-(4-quinozolin-2-yl-[1,4]diazepan-1-yl)-methanone (**41**) as a potential imaging agent (Figure 4.4). Compound **41** has a similar structure to another orexin receptor antagonist **42** ($IC_{50} < 100$ nM). Compounds **42** and **36** are both substituted diazepane orexin receptor antagonists developed by Merck & Co. Pharmaceuticals, as previously described in section 4.1.3. As shown in Figure 4.4, compound **41** reserves the significant parts of this class of orexin receptor antagonists for binding activities, such as amide carbonyl and the aromatic rings. It is proposed that compound **41** may have a similar binding affinity to that of **36** and **42**.

Unlike the radionuclide gallium-68, fluorine-18 does not require a chelator when attaching it to the targeting entity. It can be incorporated into **41** directly through nucleophilic fluorination (Figure 4.5). Without the bulky chelator, fluorine-18 may have

less of a negative effect on the binding activity as compared to the effect of a ^{68}Ga-chelator complex.
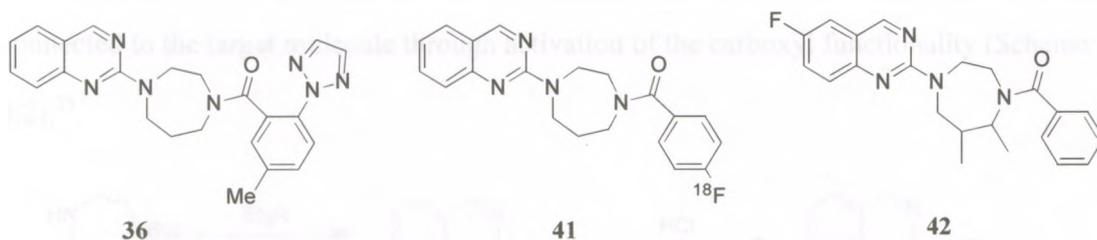

Figure 4.4 The structures of compounds **36**, **41** and **42**. Compounds **36** and **42** belong to the same class of substituted diazepane orexin receptor antagonists.


**Figure 4.5** Design of orexin receptor antagonist as an imaging agent.

4.3 Results and Discussion

The potential imaging agent **41** could be made by the coupling reaction between 2-[1,4]diazepan-1-yl-quinazoline (**46**) and [^{18}F]fluorobenzoic acid **(18)**. Since compound **41**

was designed based on the modification of **42**, the synthesis of **41** was similar to that reported for **42**. The general synthetic procedure is provided in Scheme 4.1.[34] [^{18}F]fluorobenzoic acid (**47**) could be synthesized from a (4-ethoxycarbonyl-phenyl)-trimethyl-ammonium precursor (**48**) by nucleophilic aromatic substitution and be connected to the target molecule through activation of the carboxyl functionality (Scheme 4.2).[35]
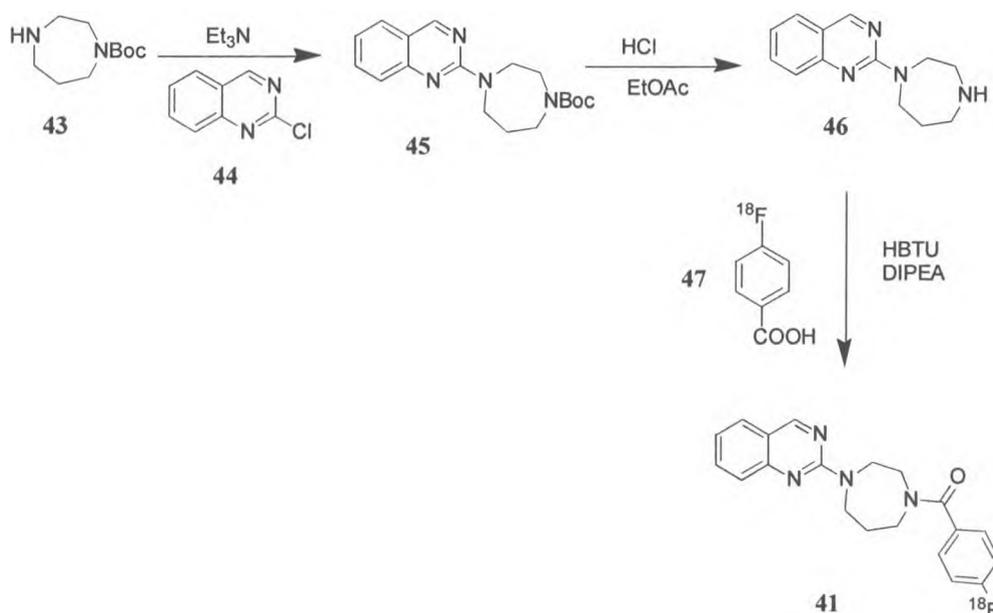

Scheme 4.1 General synthetic procedure of **41**.[34]
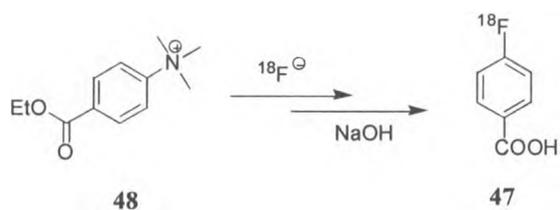
Scheme 4.2 The synthesis of compound **47**.[35]

One of the critical steps for making **41** was to make 2-chloro-quinazoline (**44**). The first approach attempted to make **44** is shown in Scheme 4.3 and follows a method reported in a patent.[36]
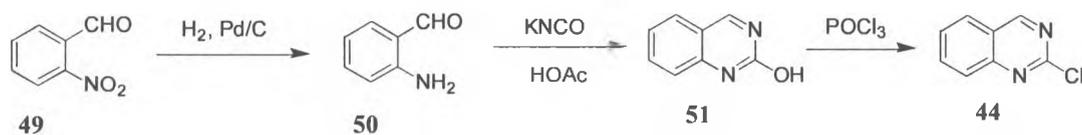
Scheme 4.3 The synthetic route of 2-chloro-quinazoline (**44**).[36]

As shown in Scheme 4.3, the first step was reducing 2-nitro-benzaldehyde (**49**) to 2-amino-benzaldehyde (**50**). The reduction of the nitro group was attempted by a catalytic hydrogenation reaction with 5% and 10% Pd/C as catalyst respectively. However, multiple products were formed after hydrogenation. One by-product was 2-amino-benzyl alcohol (**52**), which was characterized by NMR and Mass spectrometry (Figure 4.6). The two hydrogen atoms of the amino group had different chemical shifts, which might be resulted from the hydrogen bonding between –OH and –NH$_2$. Among the by-products, another two were separated as a mixture. One of them was **50** based on the data from the ^{1}H NMR spectrum (Figure 4.7). To avoid the over-reduction of **49**, the aldehyde group was protected by ethylene glycol to form 2-(2-nitrophenyl)-1,3-dioxolane (**53**) with a yield of 80% (Scheme 4.4). However, there were still multiple products formed when **53** was subjected to catalytic hydrogenation.
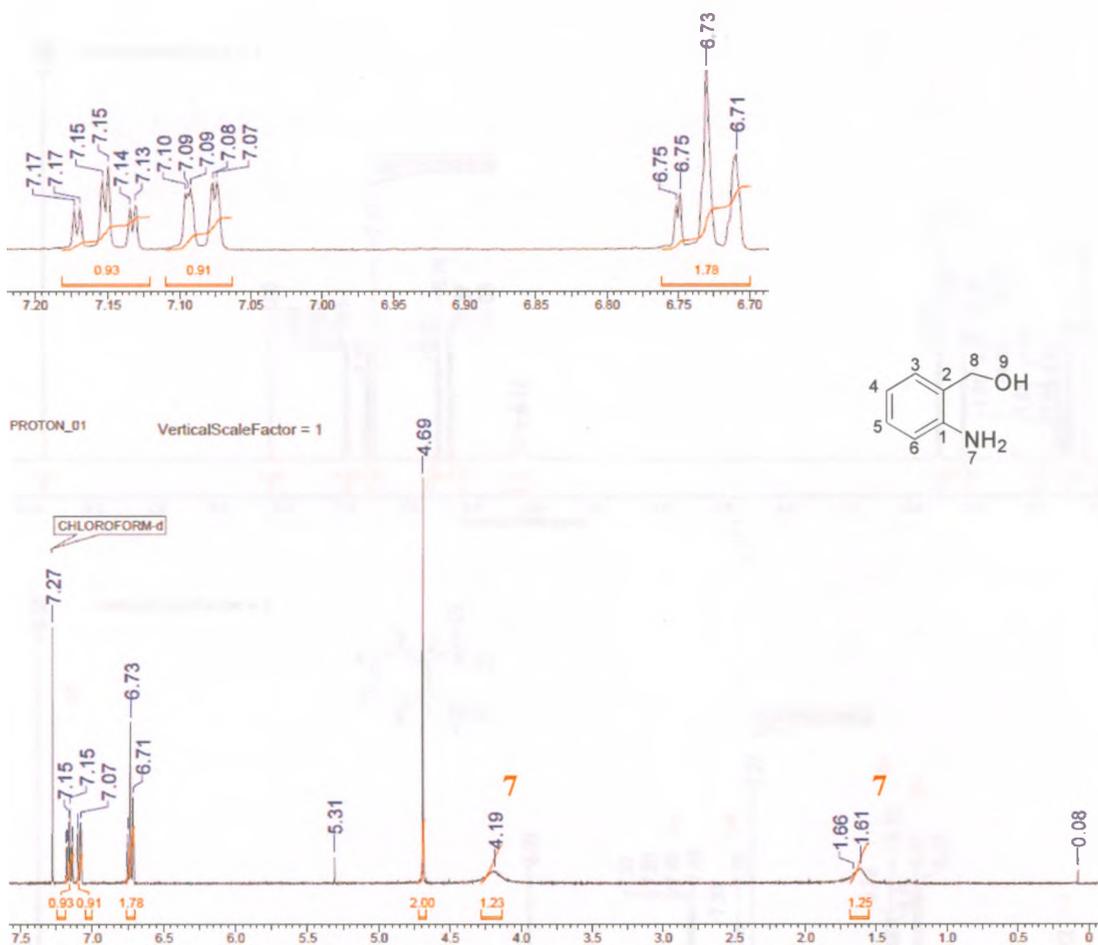
Figure 4.6 The ^{1}H NMR spectrum of a by-product 2-amino-benzyl alcohol (**52**).
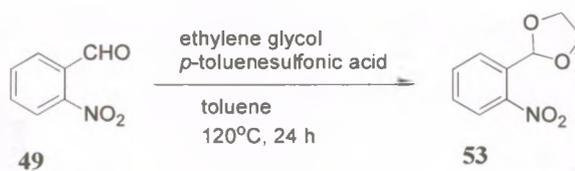
Scheme 4.4 The synthetic procedure of compound **53**.

Since the ... approach of making **44** did not work well, a second approach was attempted, as published in a Merck & Co. Pharmaceuticals patent (Scheme 4.5).[34] In order to avoid the over-reduction of compound **49**, the aldehyde functionality was protected by n-butanol before the catalytic hydrogenation reaction.
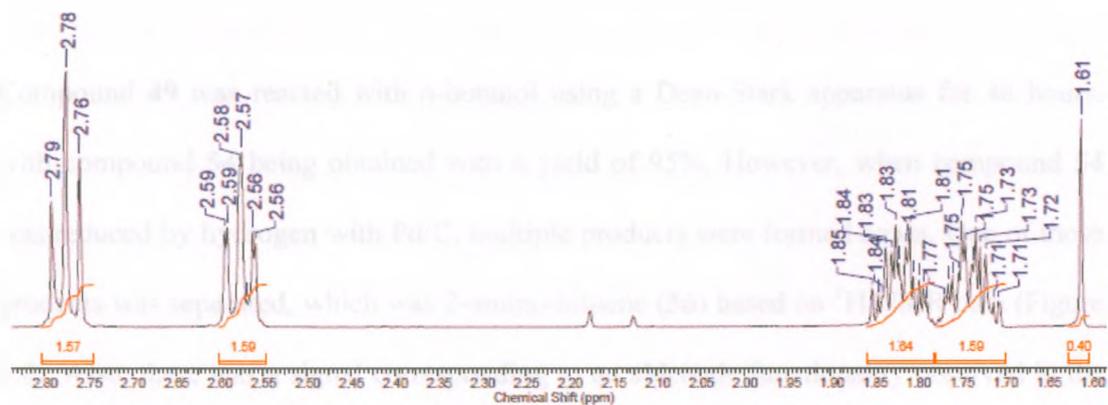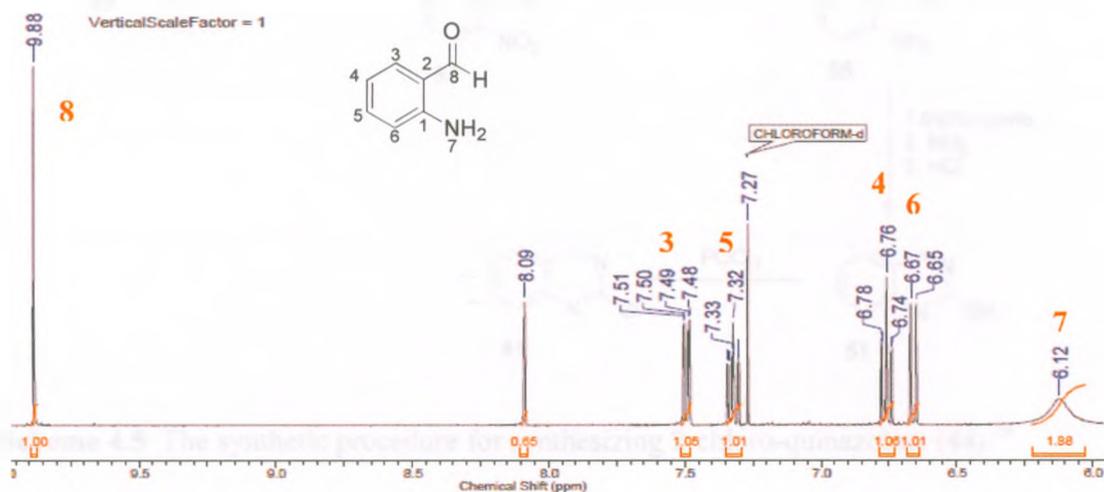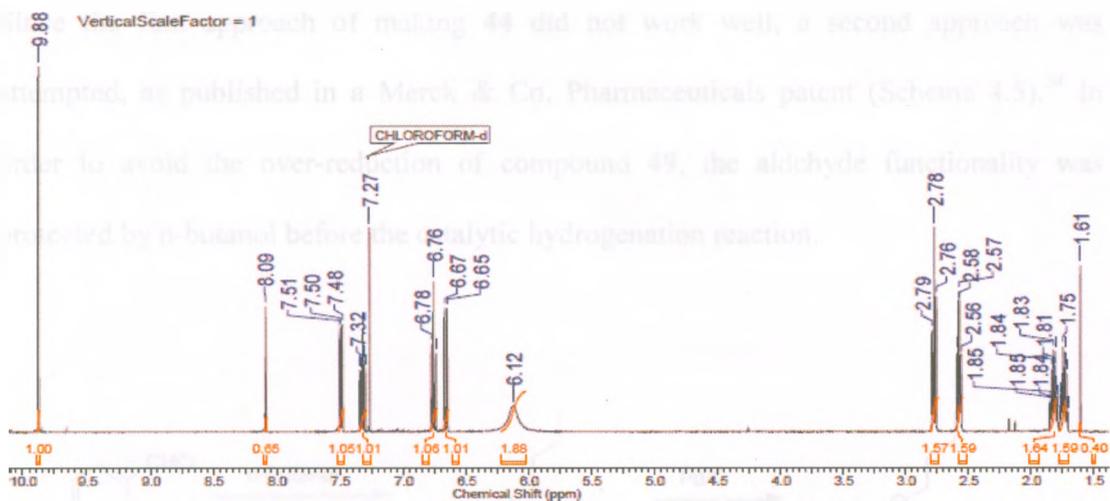
Figure 4.7   The ¹H NMR spectrum of the mixture: **50** and a by-product.

Since the first approach of making **44** did not work well, a second approach was attempted, as published in a Merck & Co. Pharmaceuticals patent (Scheme 4.5).[34] In order to avoid the over-reduction of compound **49**, the aldehyde functionality was protected by n-butanol before the catalytic hydrogenation reaction.
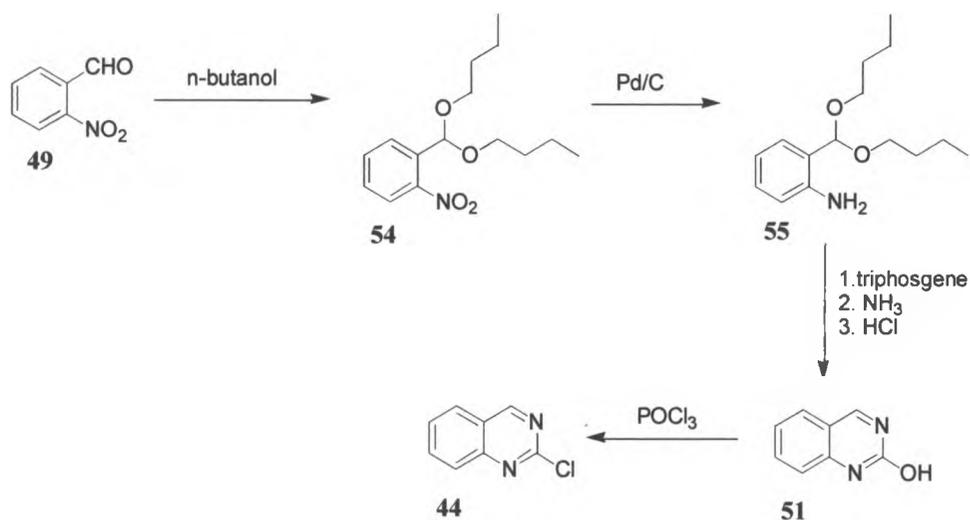
Scheme 4.5 The synthetic procedure for synthesizing 2-chloro-quinazoline (**44**).[34]

Compound **49** was reacted with n-butanol using a Dean-Stark apparatus for 48 hours, with compound **54** being obtained with a yield of 95%. However, when compound **54** was reduced by hydrogen with Pd/C, multiple products were formed again. One of those products was separated, which was 2-amino-toluene (**56**) based on ^{1}H NMR data (Figure 4.8). Also, there was a signal corresponding to an aldehyde functionality observed in the ^{1}H NMR spectrum of the crude products. Therefore, the protecting group appears to have been removed and was not stable under Pd/C hydrogenation conditions.
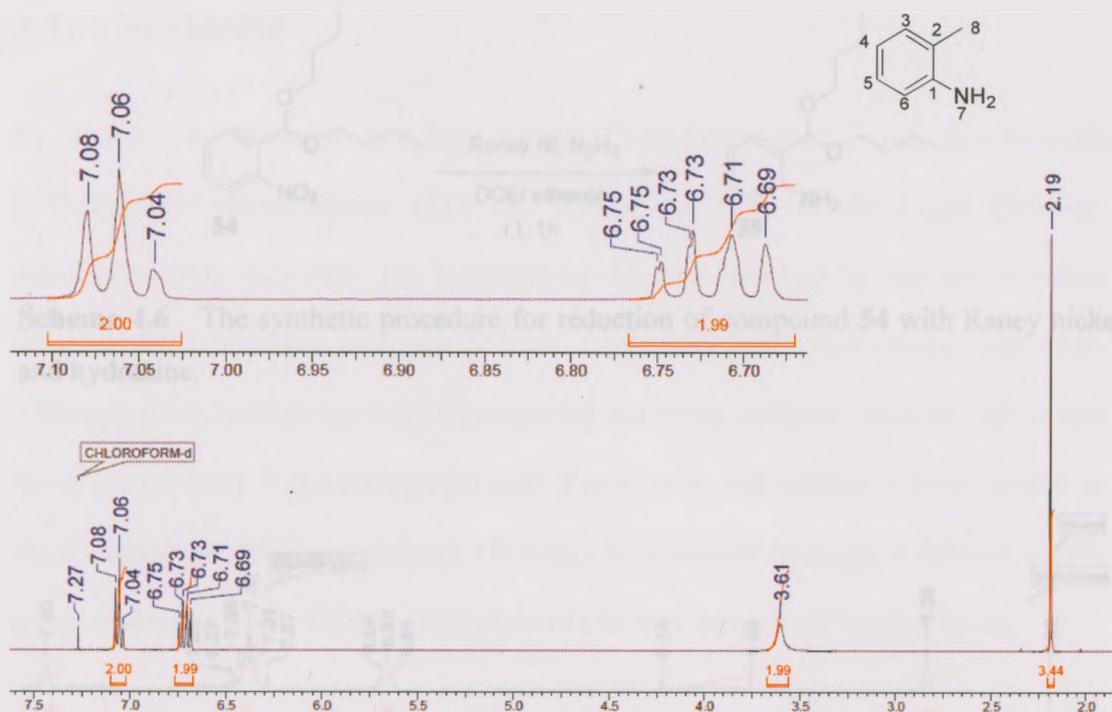
Figure 4.8 The ^{1}H NMR spectrum of by-product 2-amino-toluene (**56**).

To avoid the deprotection of the aldehyde functionality, a mild reducing agent hydrazine/Raney nickel was attempted to reduce the nitro group to an amino group (Scheme 4.6). Unexpectedly, there were three products formed and they had similar polarity. One product was the desired compound **55** with a yield of 20%. As shown in the ^{1}H NMR spectrum of **55**, the amino group had two signals (Figure 4.9). One hydrogen atom of the amino group might interact with the oxygen atom of the dibutoxymethyl group by hydrogen bonding to form a six-member ring.
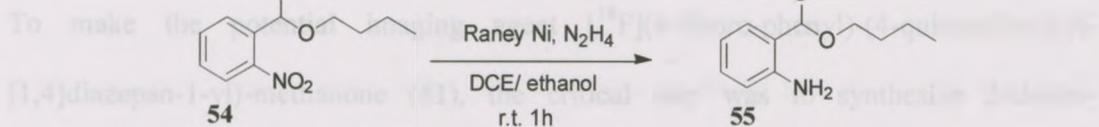
Scheme 4.6 The synthetic procedure for reduction of compound **54** with Raney nickel and hydrazine.
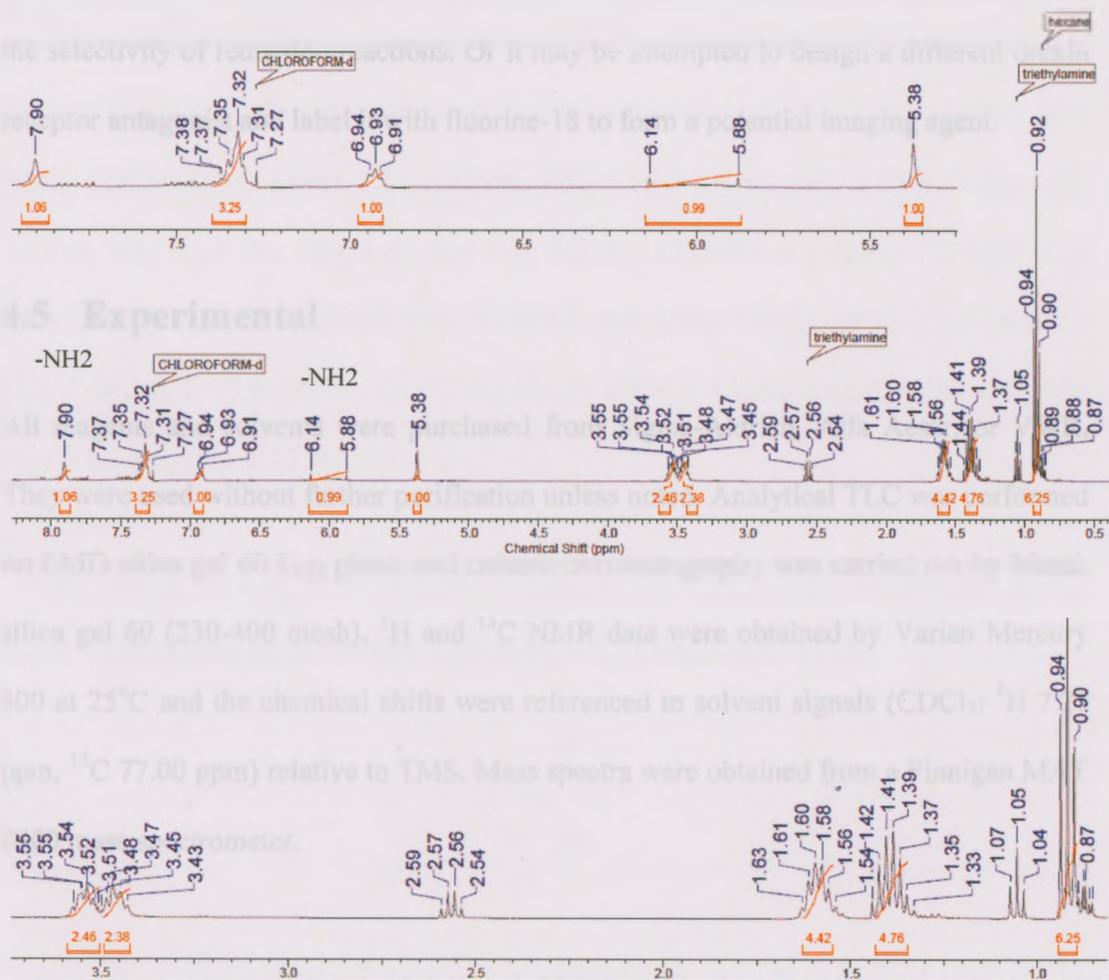

Figure 4.9 The ^{1}H NMR spectrum of 2-amino-dibutoxymethyl-benzene (**55**).

4.4 Conclusion

To make the potential imaging agent [^{18}F](4-fluoro-phenyl)-(4-quinozolin-2-yl-[1,4]diazepan-1-yl)-methanone (**41**), the critical step was to synthesize 2-chloro-quinazoline (**44**). However, the synthesis of **44** was hindered by the non-selective reduction of 2-nitro-benzaldehyde (**49**) or 1-(dimethoxymethyl)-2-nitrobenzene (**54**). Although the reduction reactions were carried out using different reducing agents and reaction conditions, it did not proceed well. Future work will require an improvement in the selectivity of reduction reactions. Or it may be attempted to design a different orexin receptor antagonist and label it with fluorine-18 to form a potential imaging agent.

4.5 Experimental

All reagents and solvents were purchased from Sigma-Aldrich, Alfa Aesar, or VWR. They were used without further purification unless noted. Analytical TLC was performed on EMD silica gel 60 F_{254} plates and column chromatography was carried out by Merck silica gel 60 (230-400 mesh). ^{1}H and ^{13}C NMR data were obtained by Varian Mercury 400 at 25°C and the chemical shifts were referenced to solvent signals (CDCl$_3$: ^{1}H 7.27 ppm, ^{13}C 77.00 ppm) relative to TMS. Mass spectra were obtained from a Finnigan MAT 8200 mass spectrometer.

4.5.1 Synthesis of 2-Amino-benzaldehyde (50)
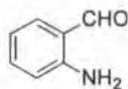
50

0.151 g 2-nitro-benzaldehyde (**49**) (1.0 mmol) was dissolved in 2 mL DCM and 2 mL MeOH, followed by adding 15.1 mg 10% Pd-C (10% wt). The mixture was stirred for 4 hours under hydrogen at room temperature. Pd-C was filtered off and the filtrate was collected. The filtrate was concentrated by evaporating off the solvents DCM and MeOH by the rotary evaporator to get a light yellow oil. The crude product was purified by column chromatography (10% EtOAc in hexane, 1% triethylamine). The yield of the by-product **52** is 15.5%. Data for the by-product 2-amino-benzyl alcohol (**22**): ^{1}H NMR (400 HMz, CDCl$_3$, 25°C) δ/ppm 7.17-7.13 (m, 1H), 7.10-7.07 (m, 1H), 6.75-6.71 (m, 2H), 4.69 (s, 2H), 4.19 (bs, 1H), 1.61 (bs, 1H); MS-EI: 123.0685 m/z (calc: 123.0684m/z). Data for 2-amino-benzaldehyde (**50**): ^{1}H NMR (400 MHz, CDCl$_3$, 25°C) δ/ppm 9.88 (s, 1H), 7.49 (dd, J = 7.8, 1.6 Hz, 1H), 7.32 (ddd, J= 8.3, 6.9, 1.6 Hz, 1H), 6.76 (m, 1H), 6.66 (d, J = 8.2 Hz, 1H), 6.12 (bs, 1H).

### 4.5.2   Synthesis of 2-(2-Nitro-phenyl)-[1,3]dioxolane (53)
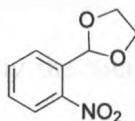
53

A solution of **49** (0.15 g, 1.0 mmol), *p*-toluenesulfonic acid monohydrate (0.02 g, 0.1 mmol) and ethylene glycol (0.19 g, 3.0 mmol) was refluxed in toluene (10 mL) with a

Dean-Stark apparatus for 24 hours. The reaction was cooled to room temperature and then the solvent was evaporated off by the rotary evaporator. The crude was purified by column chromatography (10% EtOAc in hexane) to obtain 0.16 g of 2-(2-nitro-phenyl)-[1,3]dioxolane (**53**) as a light yellow oil. The yield was 82.1%. Data for **53**: ^{1}H NMR (400 HMz, CDCl₃, 25°C) δ/ppm 7.86 (dd, J = 8, 1 Hz, 1H), 7.77 (dd, J = 7.8, 1.2 Hz, 1H), 7.61-7.57 (m, 1H), 7.49-7.45 (m, 1H), 6.45 (s, 1H), 4.04-3.96 (m, 4H). ^{13}C NMR (400 HMz, CDCl₃, 25°C) δ/ppm 148.60, 132.97, 132.70, 129.47, 127.42, 124.16, 99.33, 65.10. MS-EI ([M-H]⁺): 194.0451 m/z (calc: 194.0454 m/z).

4.5.3 Synthesis of 1-(Dimethoxymethyl)-2-nitrobenzene (54)

54
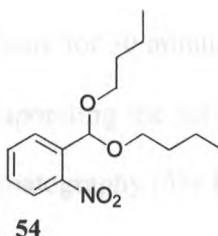
A solution of **49** (1.51 g, 10 mmol), *p*-toluenesulfonic acid monohydrate (0.20 g, 0.1 mmol) and ethylene glycol (2.53 g, 40 mmol) was refluxed in toluene (40 mL) with a Dean-Stark apparatus for 48 hours. The reaction was cooled to room temperature and then the solvent was evaporated off by the rotary evaporator. The crude material was purified by column chromatography (10% EtOAc in hexane) to obtain 2.68 g **54** as a light yellow oil. The yield was 95.4%. Data for **54**: ^{1}H NMR (400 HMz, CDCl₃, 25°C) δ/ppm 7.83-7.79 (m, 2H), 761-7.57 (m, 1H), 7.47-7.43 (m, 1H), 6.03 (s, 1H), 3.66-3.60 (m, 2H), 3.54-3.49 (m, 2H), 1.63-1.55 (m, 4H), 1.43-1.34 (m, 4H), 0.91 (t, J = 8 Hz, 1H). [13]C

NMR (400 HMz, CDCl$_3$, 25°C) δ/ppm 148.94, 133.65, 132.34, 129.04, 127.99, 124.05, 98.34, 67.48, 31.69, 19.28, 13.79. MS-EI ([M-C$_4$H$_9$O]$^+$): 208.4 m/z (calc: 208.1 m/z).

4.5.4 Synthesis of 2-Dibutoxymethyl-phenylamine (55)

55
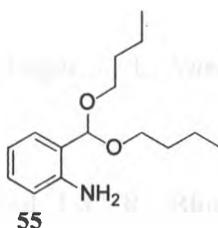
To a solution of **54** (0.84 g, 3.0 mmol) in EtOH (10 mL) and DCE (10 mL) was added 0.15 mL Raney nickel slurry. Then 0.6 mL hydrazine was added dropwise slowly. The mixture was stirred at room temperature for 30 minutes. Raney nickel was filtered off and the filtrate was concentrated by evaporating the solvents via the rotary evaporator. The crude was purified by column chromatography (5% EtOAc in hexane, 1% triethylamine) to obtain 0.15 g **55** with a yield of 19.9%. Data for 2-dibutoxymethyl-phenylamine **55**: ^{1}H NMR (400 HMz, CDCl$_3$, 25°C) δ/ppm 7.89 (s, 1H), 7.36-7.30 (m, 3H), 6.93-6.90 (m, 1H), 6.00 (bs, 1H), 5.36 (s, 1H), 3.57-3.52 (m, 2H), 3.48-3.43 (m, 2H), 1.63-1.54 (m, 4H), 1.44-1.35 (m, 4H), 0.92 (t, J = 8 Hz, 6H). MS-EI ([M]$^+$): 251.1877 m/z (calc: 251.1885 m/z).

References

(1)   Sakurai,T.; Amemiya, A.; Ishii, M; Matsuzaki, I; Chemelli, R. M.; Tanaka, H. et al. *cell* **1998**, *92*, 537.

(2)   Oomura, Y. In *Handbook of the Hypothalamus*; Morgane, P. J.; Panksepp, J., Ed., Marcel Dekker: New York, 1980.

(3)   Bernardis, L. L.; Bellinger, L. L. *Nueroscience & Biobehavioral Reviews* **1993**, *17*, 141.

(4)   Bernardis, L. L.; Bellinger, L. L. *Nueroscience & Biobehavioral Reviews* **1996**, *20*, 189.

(5)   Rodgers, R. J.; Halford, J. C. R.; Blundell, J. E. *Neuropeptides* **2002**, *36*, 303.

(6)   Sakurai, T. *Nature Reviews* **2007**, *8*, 171.

(7)   Peyron, C.; Faraco, J.; Rogers, W.; Ripley, B.; Overeem, S; Charnay, Y. et al. *Nature Medicine* **2000**, *6*, 991.

(8)   Thannickal, T. C.; Moore, R. Y.; Nienhuis, R.; Ramanathan, L.; Gulyani, S.; Aldrich, M. et al. *Neuron* **2000**, *27*, 469.

(9)   Chemelli, R. M.; Willie, J. T.; Sinton, C. M.; Elmquist, J. K.; Scammell, T.; Lee, C. et al. *Cell* **1999**, *98*, 437.

(10)   Lin, L.; Faraco, J.; Li, R.; Kadotani, H.; Rogers, W.; Lin, X. *Cell* **1999**, *98*, 365.

(11)   Hara, J.; Beuchmann, C. T.; Nambu, T.; Willie, J. T.; Chemelli, R. M.; Sinton, C. M. *Neuron* **2001**, *30*, 345.

(12)   Mignot, E.; Nevsimalova, S.; Harch, J. *Archives of Neurology* **2002**, *59*, 1553.

(13)   The International Classification of Sleep Disorders: Diagnostic and Coding Manual. *American Academy of Sleep Medicine* 2005.

(14)   Sakurai, T. In *The Orexin/Hypocretin System: Physiology and Pathophysiology*; Nishino, S.; Sakurai, T., Ed.; Humana Press: Totowa, 2006.

(15)   Cai, J. Q.; Cooke, F. E.; Sherborne, B. S. *Expert Opinions on Therapeutic Patents* **2006**, *16*, 631.

(16)   Coleman, P. J.; Renger, J. J. *Expert Opinions on Therapeutic Patents* **2010**, *20*, 307.

(17)   Smart, D.; Sabido-David, C.; Brough, S. J.; Jewitt, F.; Johns, A.; Porter, R. A. et al. *British Journal of Pharmacology* **2001**, *132*, 1179.

(18)   Haynes, A. C.; Chapman, H.; Taylor, C.; Moore, G. B. T.; Cawthorne, M. A.; Tadayyon, M., et al. *Regulatory Peptides* **2002**, *104*, 153.

(19)   Cox, C. D.; Breslin, M. J.; Whitman, D. B.; Schreier, J. D.; McGaughey, G. B.; Bogusky, M. J. et al. *Journal of Medicinal Chemistry* **2010**, *53*, 5320.

(20)   Roecher, A.J.; Coleman, P. J. *Current Topics in Medicinal Chemistry* **2008**, *8*, 977.

(21)   Brisbare-Roch, C.; Dingemanse, J.; Koberstein, R.; Hoever, P.; Aissaoui, H; Flores, S. et al. *Nature Medicine* **2007**, *13*, 150.

(22)   Meck   2008   Business   Briefing-Final. http://goliath.ecnext.com/coms2/gi_0199-9773483/Merck-2008-Annual-Business Briefing.html.

(23)   Bergman, J.; Coleman, P. J.; Cox, C. D.; Roecker, A. J. U.S. Patent US2008/012182, May 07, 2009.

(24)   Coleman, P. J.; Schreier, J. D.; McGaughey, G. B.; Bogusky, M. J.; Cox, C. D.; Hartman, G. D. et al. *Bioorganic and Medicinal Chemistry Letters* **2009**, *19*, 2997.

(25)   Snyder, S. E.; Kilbourn, M. R. In *Handbook of Radiopharmaceuticals: Radiochemistry and Applications*; Welch, M. J.; Redvanly, C. S., Ed.; John Wiley & Sons: West Sussex, 2003.

(26)   O'Hagan, D. *Chemical Society Reviews* **2008**, *37*, 308.

(27)   Rentmeister, A.; Arnold, F. H.; Fasan, R. *Nature Chemical Biology* **2009**, *5*, 26.

(28)   Som, P.; Atkins, H. L. *Journal of Nuclear Medicine* **1980**, *21*, 670.

(29)   Weber, G. *New England Journal of Medicine* **1977**, *296*, 541.

(30)   Kantorova, I.; Lipska, L.; Belohlavek, O.; Visokai, V.; Trubac, M.; Schneiderova, M. *Journal of Nuclear Medicine* **2003**, *44*, 1784.

(31)   Schiepers, C.; Valk, P. E. In *Positron Emission Tomography: Clinical Practice*; Valk, P. E.; Delbeke, D.; Bailey, D. L.; Townsend, D. W.; Maisey, M. N., Ed.; Springer-Verlag: London, 2006.

(32)   Strauss, L. G. *European Journal of Nuclear Medicine* **1996**, *23*, 1409.

(33)   Rouet-Benzineb, P.; Rouyer-Fessard, C.; Jarry, A.; Avondo, V.; Pouzet, C.; Yanagisawa, M. *The Journal of Biological Chemistry* **2004**, *279*, 45875.

(34)   Bergman, J.; Coleman, P. J.; Cox, C. D.; Roecker, A. J. WIPO WO 2009/058238 A1, May 07, 2009.

(35)   Marik, J.; Sutcliff, J. L. *Applied Radiation adn Isotopes* **2007**, *65*, 199.

(36)   Iwakuni, K.Y.; Kuga, K. K.; Ohtake, T. K.; Iwakuni, H. O.; Nishina, T.; Kumakura, M. et al. U.S. Patent 4734418, March 29, 1988.

Chapter 5   Conclusion and Outlook

According to World Health Organization statistics, cancer is still the leading cause of death in the world and 7.6 million people (around 13% of all deaths) died of cancer in 2008.[1] However, the cancer mortality rate is dropping by about one percent annually and the five-year survival rate is increasing, which reflects an improvement in the early diagnosis and effective treatment of cancer.[2] This improvement is partially a result of the application of molecular imaging techniques in cancer diagnostics. Molecular imaging provides biological information in a human body at the molecular and cellular level, noninvasively. Through molecular imaging techniques, cancer can be detected in its early stage before abnormalities can be identified with other diagnostic tests.[2] The potential significance of molecular imaging in cancer diagnosis leads to the work presented in this thesis, in the design of orexin receptor agonists and antagonists as potential imaging probes targeting colon cancer cells.

The first research project focused on designing orexin agonists orexin A (33 amino acids) and orexin B (28 amino acids) as potential imaging agents targeting colon cancer cells, in which orexin receptor 1 (OX$_1$R) is expressed. Because of favourable biodistribution patterns of small peptides, the analogues of orexin A and orexin B, orexin A (15-33) and orexin B (6-28), were developed as potential imaging agents. The N-terminal residues of orexin peptides are much less significant for biological binding affinities than the C-terminal residues, allowing for attachment of imaging labels to orexin peptides through the N-terminal residues.

First of all, orexin A (15-33) and orexin B (6-28) were labelled with fluorescein isothiocyanate (FITC) for a preliminary cell study *in vitro*. A linker amino hexanoic acid (Ahx) was used between the orexin peptide and the imaging label FITC to reduce the bulky effects of the imaging label on binding affinities. Due to the poor solubility of FITC-Ahx-orexin A (15-33) (**1**) and FITC-Ahx-orexin B (6-28) (**3**), an AEEA linker was used instead of Ahx, and the solubility of FITC-AEEA-orexin A (15-33) (**2**) and FITC-AEEA-orexin B (6-28) (**4**) was slightly improved.

A shallow penetration depth limits the use of FITC as an imaging label for animal studies *in vivo*, which leads to the design of gallium-68 radiolabelled orexin peptides. Gallium-68 cannot be introduced into orexin peptides directly. Therefore a bifunctional chelator DOTA was conjugated to orexin peptides, and then coordinated with gallium-68 during the radiolabelling process. Orexin A (15-33) and orexin B (6-28) were successfully radiolabelled with gallium-68 via the ^{68}Ge/^{68}Ga generator system to get two imaging agents ^{68}Ga-DOTA-Ahx-orexin A (15-33) (**8**) and ^{68}Ga-DOTA-Ahx-orexin B (6-28) (**11**), which may be used for PET imaging. The nonradioactive Ga-DOTA-Ahx-orexin A (15-33) (**12**) and Ga-DOTA-Ahx-orexin B (6-28) (**13**) were synthesized as well to study their binding affinities to OX_1R. Their IC_{50} values were 629 nM and 168 nM respectively.

The second research project focused on synthesizing a potential orexin receptor antagonist **41** and radiolabelling it with fluorine-18 to get an imaging probe targeting

colon cancer cells. The synthesis of **41** was not completed. Future work may improve the selectivity of the reduction reaction which hindered the progress of the synthetic work, or develop a new potential orexin receptor antagonist based on published structures of antagonists that were reported to have high binding affinities.

Since the orexin family was discovered in 1998, much research has been done to develop orexin receptor agonists and antagonists as potential drugs to treat sleep disorder and obesity. However, this thesis presents another promising application of orexin receptor agonists and antagonists in the molecular imaging area. Hopefully, the imaging agents based on orexin agonists or antagonists can be developed successfully in the future and will play a role in the early detection of colon cancer to increase the survival rate of cancer patients.

References

(1)   World Health Organization. http://www.who.int/mediacentre/factsheets/fs297/en/.

(2)   Center for Molecular Imaging Innovation and Translation. http://www.molecularimagingcenter.org/index.cfm?PageID=9702.

Appendix

HPLC and ESI-MS Spectra of Fluorescein-Ahx-Orexin A (15-33) (1)

ZL-1-037-5-analytical_30to60_15min_vydac-2   2: Diode Array
12.40 Range: 1.549e+1

ZL-2-101-2-INFUSION 36 (0.665) Cm (16:44)   Scan ES+
841.45   1.74e7

636.73
631.25
848.79
1261.66
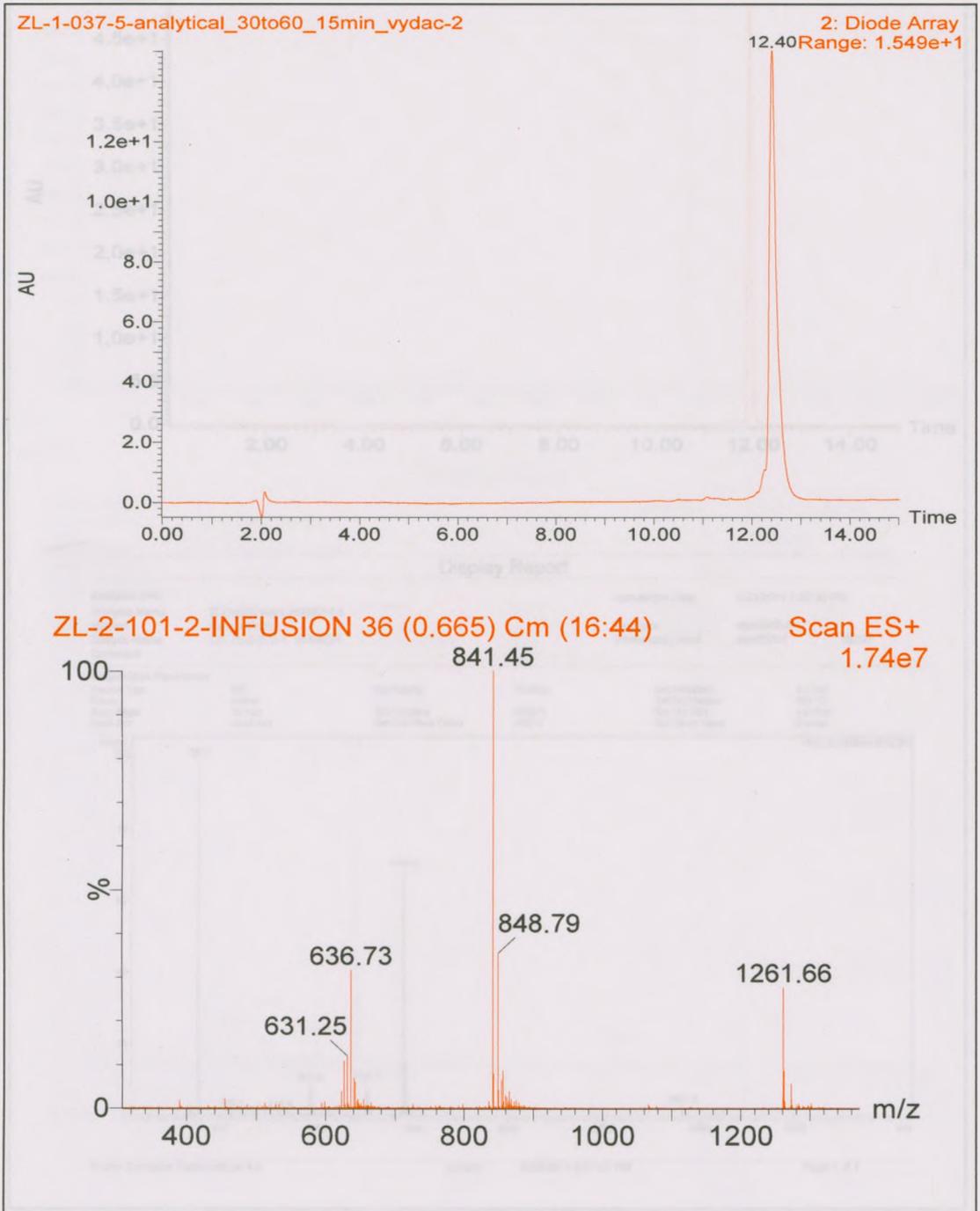
HPLC and ESI-MS Spectra of Fluorescein-Ahx-Orexin B (6-28) (3)

# HPLC and ESI-MS Spectra of Ga-DOTA-Ahx-Orexin A (15-33) (12)

# HPLC and ESI-MS Spectra of Ga-DOTA-Ahx-Orexin B (6-28) (13)

¹H-NMR Spectrum of [2-[2-(Fmoc-amino) ethoxy] ethoxy]-ethanol (29)

29
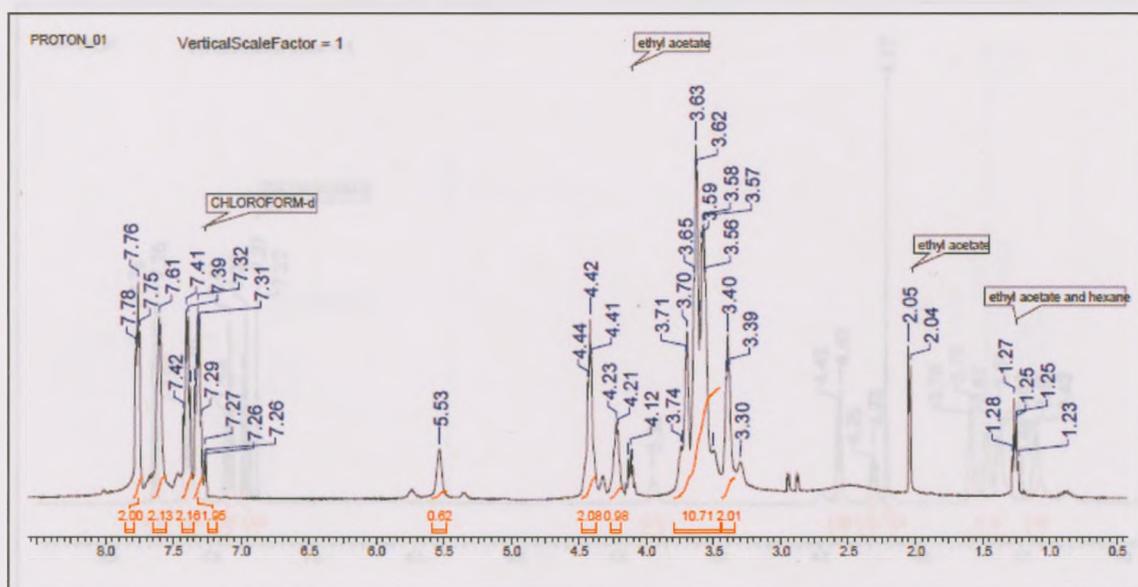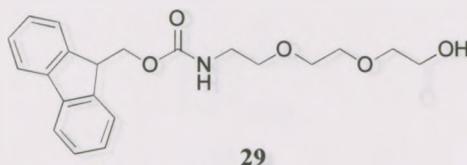
# ^{1}H-NMR and ^{13}C-NMR Spectra of [2-(2-Amino-ethoxy)-ethoxy]-acetic acid (24)

24
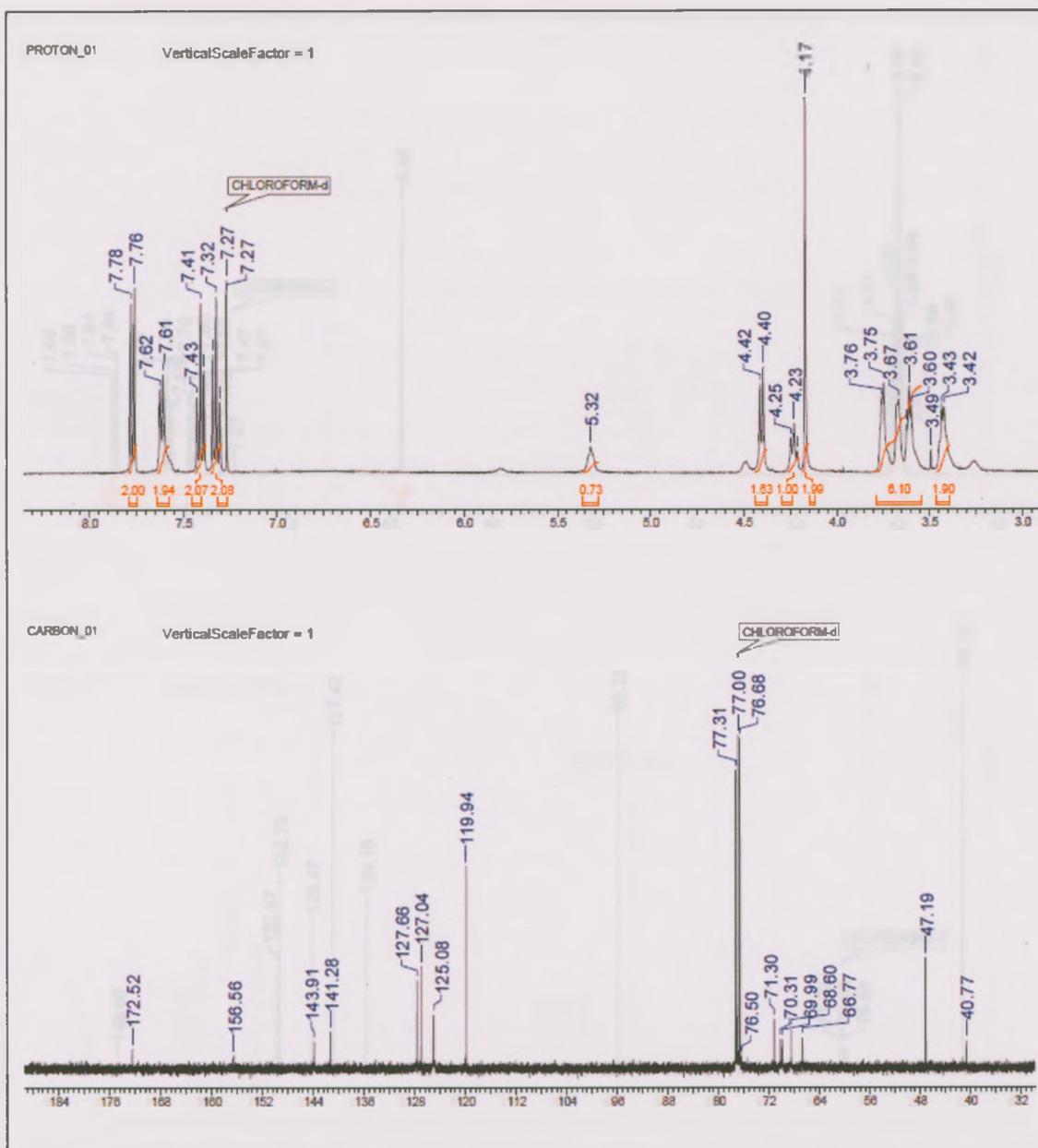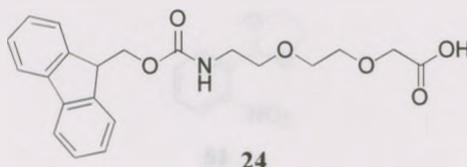
^{1}H-NMR and ^{13}C-NMR Spectra of 2-(2-Nitro-phenyl)-[1,3]dioxolane (53)
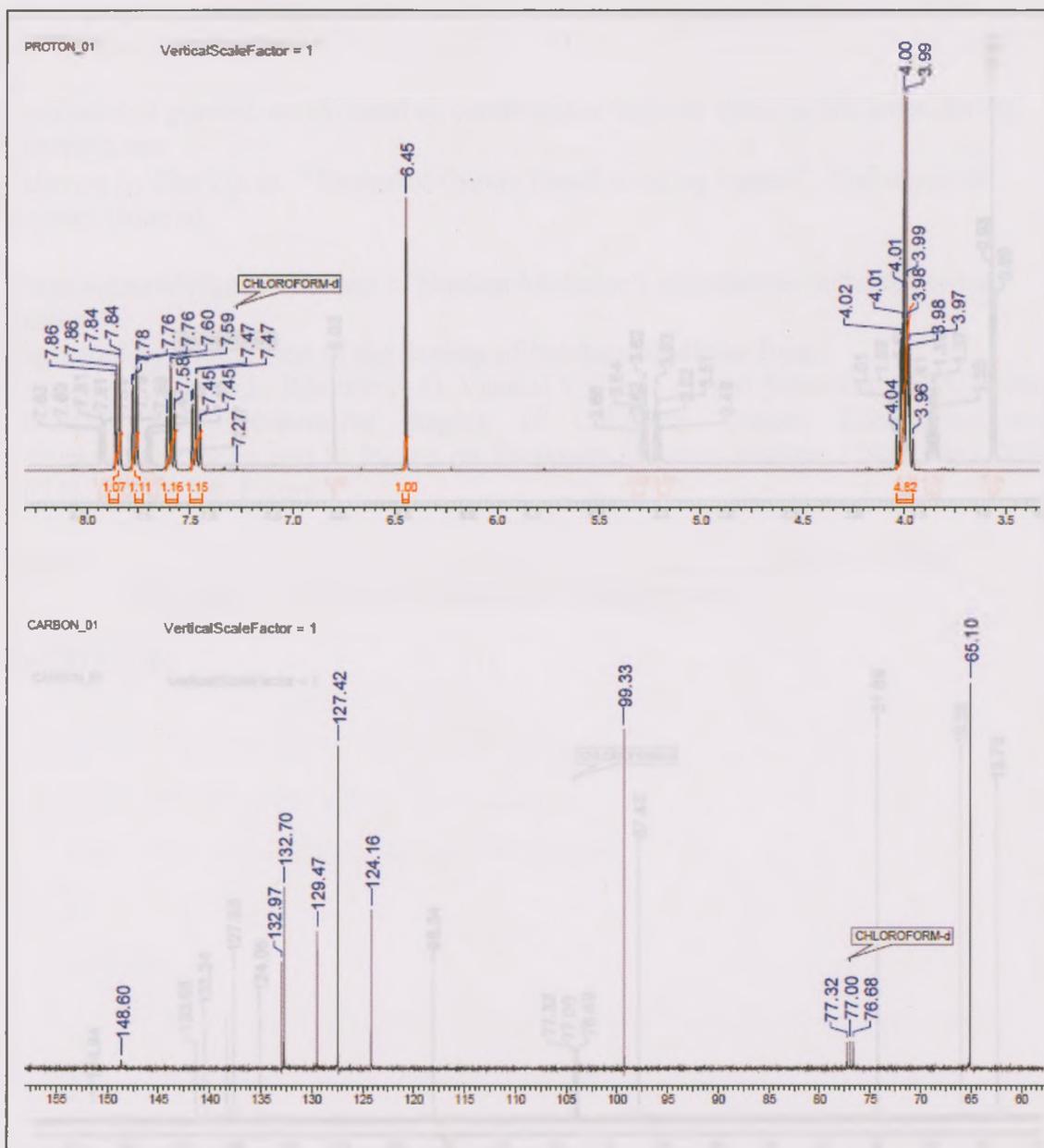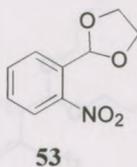
^{1}H-NMR and ^{13}C-NMR Spectra of 2-Dibutoxymethyl-phenylamine (55)

55

PROTON_01   VerticalScaleFactor = 1

0.91
0.93
0.89
CHLOROFORM-d
6.03
3.66 3.64 3.62 3.53 3.52 3.51 3.49 3.62
7.83 7.83 7.81 7.81 7.79 7.79 7.59 7.47 7.45 7.45 7.27
1.61 1.59 1.57 1.41 1.39 1.37 1.36 1.62
1.93 1.02 1.00   1.00   2.08 2.26   4.21 4.19   6.04

8.0 7.5 7.0 6.5 6.0 5.5 5.0 4.5 4.0 3.5 3.0 2.5 2.0 1.5 1.0 0.5

CARBON_01   VerticalScaleFactor = 1

31.69
19.28
13.79
CHLOROFORM-d
67.48
98.34
148.94 133.65 132.34 127.99 124.05
77.32 77.00 76.69

152 144 136 128 120 112 104 96 88 80 72 64 56 48 40 32 24 16 8

94

SNM

Advancing Molecular Imaging and Therapy

July 15, 2011
Zhu Lin

Dear Zhu Lin:

Thank you for your request to reprint material from a Society of Nuclear Medicine publication.

Permission is granted, conditioned on conformance with the terms in this letter, for the following use:
Inclusion by Zhu Lin in "Design of Orexin Based Imaging Agents" (University of Western Ontario).

Please acknowledge the Society of Nuclear Medicine's contribution in the following manner:
Reprinted by permission of the Society of Nuclear Medicine from:
Kantorová I, Lipská L, Bêlohlávek O, Visokai V, Truba M, and Schneiderová M. Routine 18F-FDG PET Preoperative Staging of Colorectal Cancer: Comparison with Conventional Staging and Its Impact on Treatment Decision Making. J Nucl Med. 2003; 44(11): 1784-1788. Figure 1

Signed: _____Date: 7/15/2011
             Rebecca L. E. Maxey, Director of Communications

Ref: RQ01281